AD-A083 393 NAVAL RESEARCH LAB WASHINGTON DC F/G 4/1
NONLINEAR EQUATORIAL SPREAD F: SPATIALLY LARGE BUBBLES RESULTIN--ETC(U)
FEB 80 S T ZALESAK, S L OSSAKOW
UNCLASSIFIED NRL-MR-4154 SBIE-AD-E000 391 NL

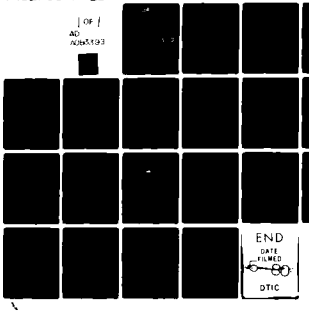

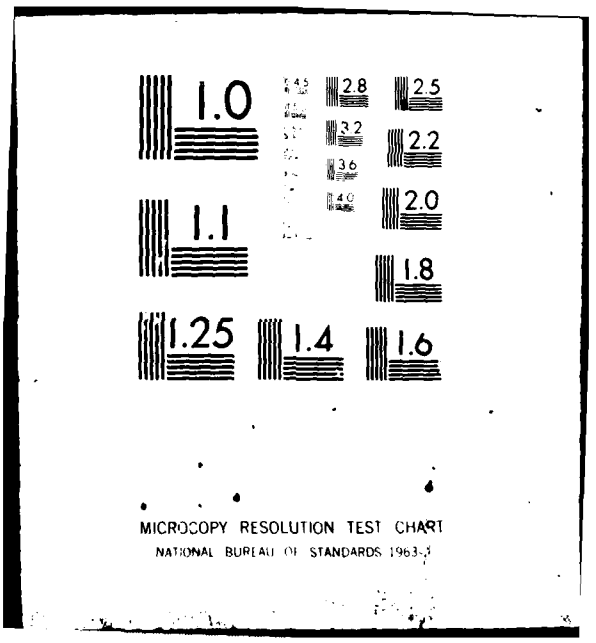
1.0
2.8
2.5
3.2
2.2
3.6
2.0
4.0
1.1
1.8
1.25
1.4
1.6
MICROCOPY RESOLUTION TEST CHART
NATIONAL BUREAU OF STANDARDS 1963-A

NRL Memorandum Report 4154

Nonlinear Equatorial Spread F: Spatially Large Bubbles Resulting from Large Horizontal Scale Initial Perturbations

S. T. ZALESAK AND S. L. OSSAKOW

Geophysical and Plasma Dynamics Branch
Plasma Physics Division

February 6, 1980

This research was sponsored partially by the Defense Nuclear Agency under Subtask S99QAXHC041, work unit 21 and work unit title Plasma Structure Evolution; and partially by the Office of Naval Research.

NAVAL RESEARCH LABORATORY
Washington, D.C.

SECURITY CLASSIFICATION OF THIS PAGE (When Data Entered)

REPORT DOCUMENTATION PAGE

READ INSTRUCTIONS BEFORE COMPLETING FORM

1. REPORT NUMBER: NRL Memorandum Report 4154	2. GOVT ACCESSION NO. / 3. RECIPIENT'S CATALOG NUMBER
4. TITLE (and Subtitle): NONLINEAR EQUATORIAL SPREAD F: SPATIALLY LARGE BUBBLES RESULTING FROM LARGE HORIZONTAL SCALE INITIAL PERTURBATIONS	5. TYPE OF REPORT & PERIOD COVERED: Interim report on a continuing NRL problem.
	6. PERFORMING ORG. REPORT NUMBER
7. AUTHOR(s): S. T. Zalesak and S. L. Ossakow	8. CONTRACT OR GRANT NUMBER(s)
9. PERFORMING ORGANIZATION NAME AND ADDRESS: Naval Research Laboratory, Washington, DC 20375	10. PROGRAM ELEMENT, PROJECT, TASK AREA & WORK UNIT NUMBERS: NRL Problems 67-0889-0-0 and 67-0883-0-0, DNA Subtask S99QAXHCO41
11. CONTROLLING OFFICE NAME AND ADDRESS: Defense Nuclear Agency, Washington, DC 20305 and Office of Naval Research, Arlington, VA 22217	12. REPORT DATE: February 6, 1980
	13. NUMBER OF PAGES: 44
14. MONITORING AGENCY NAME & ADDRESS(if different from Controlling Office)	15. SECURITY CLASS. (of this report): UNCLASSIFIED
	15a. DECLASSIFICATION/DOWNGRADING SCHEDULE

16. DISTRIBUTION STATEMENT (of this Report)

Approved for public release; distribution unlimited.

17. DISTRIBUTION STATEMENT (of the abstract entered in Block 20, if different from Report)

18. SUPPLEMENTARY NOTES

This research was sponsored partially by the Defense Nuclear Agency under Subtask S99QAXHCO41, work unit 21 and work unit title Plasma Structure Evolution; and partially by the Office of Naval Research.

19. KEY WORDS (Continue on reverse side if necessary and identify by block number)

Nonlinear equatorial spread F
Spatially large bubbles
Collisional Rayleigh-Taylor regime
Numerical simulations

20. ABSTRACT (Continue on reverse side if necessary and identify by block number)

Motivated by the observations of large horizontal scale length equatorial spread F "bubbles", we have performed numerical simulations of the nonlinear evolution of the collisional Rayleigh-Taylor instability in the nighttime equatorial ionosphere, using large horizontal scale length initial perturbations. The calculations were performed using a new, improved numerical code which utilizes the recently developed, fully multidimensional flux-corrected transport (FCT) techniques. We find that large horizontal scale initial perturbations evolve nonlinearly into equally large horizontal scale spread F bubbles, on a time scale as fast as that of the corresponding small horizontal

(Continues)

DD FORM 1 JAN 73 1473 EDITION OF 1 NOV 65 IS OBSOLETE
S/N 0102-014-6601

SECURITY CLASSIFICATION OF THIS PAGE (When Data Entered)

20. Abstract (Continued)

scale length perturbations previously used. Further, we find the level of plasma depletion inside the large scale bubbles to be appreciably higher than that of the smaller scale bubbles, approaching 100%, in substantial agreement with the observations. This level of depletion is due to the fact that the plasma comprising the large scale bubbles has its origin at much lower altitudes than that comprising the smaller scale bubbles. Analysis of the polarization electric fields produced by the vertically aligned ionospheric irregularities show this effect to be due to fringe fields similar in structure to those produced at the edge of a parallel plate capacitor.

CONTENTS

I. INTRODUCTION

Our previous numerical simulations of the nonlinear evolution of the collisional Rayleigh-Taylor instability in the nighttime equatorial ionosphere (spread F) were confined to small (~ 3km) horizontal scale length initial perturbations and hence to fully developed spread F "bubbles" of approximately the same size in horizontal extent [Scannapieco and Ossakow, 1976; Ossakow et al., 1979], although spatially large vertically. However, observations by McClure et al [1977] also indicate ionospheric ion density "biteouts" of much larger horizontal extent (10 - > 200 km) and greater intensity (ion density depletions up to three orders of magnitude) than indicated by our small scale simulations. Therefore, we have extended our previous calculations and have performed a series of numerical simulations using much larger horizontal length scales (~ 75km) for our initial perturbations. These seed long wavelength perturbations, for example, could be due to neutral atmosphere gravity wave effects [Rottger, 1976; Klostermeyer, 1978; Booker, 1979]. At the same time we have made very substantial improvements in the numerical techniques used to perform the simulations, including the utilization of the recently developed fully multidimensional flux-corrected transport (FCT) techniques of Zalesak [1979] . The results of our simulations indicate the following:

1) large horizontal scale length initial perturbations evolve nonlinearly into large horizontal scale length equatorial spread F "bubbles;"
2) these bubbles evolve on approximately the same time scale as do their smaller horizontal scale length counterparts;

Note: Manuscript submitted December 4, 1979.

3) the plasma comprising these bubbles has its origin at much lower altitudes than that of the smaller horizontal scale length bubbles, resulting in plasma density depletions of very close to 100%.

This last result is due to the fact that the polarization fields produced by ionospheric irregularities, aligned vertically, possess a fringe field component whose vertical extent is proportional to the horizontal extent of the irregularities producing the field. This is quite similar in origin to the fringe field produced at the edge of a parallel plate capacitor. Since the vertical extent of this fringe field determines the minimum altitude from which the rising bubble can draw plasma, it is not surprising that larger horizontal scale bubbles are more severely depleted. In Section II we give a brief review of the relevant theory, and of the basic equations used in our simulations. Section III contains the numerical simulations and a physical interpretation of the results is given. Section IV contains a summary, and in the appendix we describe briefly the numerical techniques used in our present computer code, emphasizing the differences between the present code and our previous one.

II. THEORY

The geometry of the physical problem we are modeling is the same as in Ossakow et al. [1979]. All our simulations are carried out in a two dimensional (x,y) coordinate system. The constant magnetic field $\underline{B}$ is aligned along the $\hat{z}$ axis (pointing north). Gravity is directed along the negative $\hat{y}$ axis. Since our equations are two dimensional, n(y), $\nu_R(y)$, and $\nu_{in}(y)$ are taken to be representative values of the ambient electron density, recombination coefficient, and ion-neutral collision frequency (the result of integrating these quantities along magnetic field lines and dividing by a normalizing scale length). Magnetic field lines are assumed to terminate at both ends in an electrically insulated medium (currents must close in the two dimensional plane, not in some distant E region).

Following Ossakow et al. [1979], we describe the system with the two-fluid plasma continuity and momentum equations:

$$\frac{\partial n_\alpha}{\partial t} + \nabla \cdot (n_\alpha \underline{v}_\alpha) = - \nu_R n_\alpha \tag{1}$$

$$\left(\frac{\partial}{\partial t} + \underline{v}_\alpha \cdot \nabla\right) \underline{v}_\alpha = \frac{q_\alpha}{m_\alpha} \left(\underline{E} + \frac{\underline{V}_\alpha \times \underline{B}}{c}\right) + \underline{g} - \nu_{\alpha n}(\underline{v}_\alpha - \underline{U}_n) \tag{2}$$

where the subscript α denotes the species (i for ions, e for electrons), n is the species number density, $\underline{v}$ is velocity, ν_R is the recombination coefficient, $\underline{E}$ is the electric field, $\underline{g}$ is the gravitational acceleration, q is the species charge, $\nu_{\alpha n}$ is the species collision frequency with the

neutral atmosphere, $\underline{U}_n$ is the neutral wind velocity, c is the speed of light, and m is the species mass.

Note that, in contrast to Ossakow et al [1979], we have dropped the term + $\nu_R n_{\alpha o}$ from (1). This is the equivalent of dropping the assumption of the existence of an ionization source given by that term. This ionization source was such that the ambient ionization profile $n_{\alpha o}(y)$ was an equilibrium profile ($\partial n_{\alpha o}/\partial t = 0$). Our present model therefore has instead

$$\frac{\partial n_{\alpha o}}{\partial t} = - \nu_R n_{\alpha o} \tag{3}$$

Hence, when normalized results $n_\alpha(x,y)/n_{\alpha o}(y)$ are later presented, it should be understood that both the numerator and denominator are time dependent.

Figure 1 shows the recombination rate ν_R and ion-neutral collision frequency ν_{in} used in our simulations. It shall be seen presently that ν_{en} need not be specified as long as it is much smaller than the electron gyro frequency Ω_e. For details on the form of ν_{in} and ν_R as depicted in Figure 1, see Ossakow et al.[1979]. If we neglect the inertial terms (the left-hand side) of (2) by assuming the inertial time scales are much larger than either the gyro periods or the mean time between collisions, then the equation can be inverted to give an algebraic expressions for $\underline{v}_\alpha$. In two-dimensional (x,y) geometry with $\underline{B}$ along the $\hat{z}$ axis, the solution is for our problem, with $m_e \ll m_i$, $\nu_{in}/\Omega_i \ll 1$, $\nu_{en}/\Omega_e = 0$ (where $\Omega_\alpha = eB/m_\alpha c$), and $\underline{U}_n = 0$.

$$\underline{v}_e = \frac{c}{B}\ \underline{E} \times \hat{z},\ \hat{z} = \frac{\underline{B}}{|\underline{B}|} \tag{4}$$

$$\underline{v}_i = \left(\frac{\underline{g}}{\Omega_i} + \frac{c}{B}\ \underline{E} \right) \times \hat{z} + \frac{\nu_{in}}{\Omega_i} \left(\frac{\underline{g}}{\Omega_i} + \frac{c}{B}\ \underline{E} \right) \tag{5}$$

We now make the electrostatic approximation,

$$\underline{E} = \nabla_\perp \phi \tag{6}$$

where $\nabla_\perp \equiv \hat{x}(\partial/\partial x) + \hat{y}(\partial/\partial y)$, and the quasi-neutrality approximation $n_e \approx n_i \equiv n$. We then have

$$\nabla_\perp \cdot \underline{j} = 0 \tag{7}$$

$$\underline{j} \equiv en\ (\underline{v}_i - \underline{v}_e) \tag{8}$$

Substituting (4) and (5) into (8) and evaluating (7), we have for the electrostatic potential:

$$\nabla_\perp \cdot (\nu_{in} n\ \nabla_\perp \phi) = -\frac{m_i}{e}\ g\ \frac{\partial}{\partial y}\ (\nu_{in} n) - \frac{B}{c}\ g\ \frac{\partial n}{\partial x} \tag{9}$$

As in Ossakow et al. [1979] we set $\phi = \phi_o + \phi_1$ where $\nabla_\perp \phi_o = -(m_i g/e)\ \hat{y}$. Since $\nabla_\perp^2\ \phi_o = 0$, our final potential equation becomes

$$\nabla_\perp \cdot (\nu_{in}\ n\ \nabla_\perp \phi_1) = -\frac{Bg}{c}\ \frac{\partial n}{\partial x} \tag{10}$$

The effect of ϕ_o is merely to superimpose a bulk westward plasma velocity g/Ω_i on the electron velocity field determined from ϕ_1, without affecting the morphology of the developing structures. Hence, we ignore this motion.

Our assumption of quasi-neutrality has made one of our two continuity equations (1) redundant. We therefore choose the electron equation for its simplicity:

$$\frac{\partial n}{\partial t} - \frac{\partial}{\partial x}\left(\frac{nc}{B}\frac{\partial \phi_1}{\partial y}\right) + \frac{\partial}{\partial y}\left(\frac{nc}{B}\frac{\partial \phi_1}{\partial x}\right) = -\nu_R n \qquad (11)$$

III. NUMERICAL SIMULATION RESULTS AND DISCUSSION

Equations (10) and (11), together with appropriate boundary conditions, constitute the nonlinear system of equations we shall solve numerically. Note that in contrast to Ossakow et al. [1979], we have chosen not to put the equations into a normalized form by dividing through by $n_o(y)$. The numerical techniques used to solve these equations are discussed in the appendix.

The numerical calculations to be presented were performed on a two-dimensional cartesian (x,y) mesh using 42 points in the x (east-west) direction, and 142 points in the y (vertical) direction. The (uniform) grid spacing was 2km in the y direction for all calculations. The grid spacing in the x direction was 200m in the "small" horizontal scale length cases and 5km in the "large" cases. The bottom of the grid corresponds to 252km altitude and the top of the grid to 534km altitude in all simulations. Periodic boundary con-

ditions were imposed on both n and ϕ_1 in the x-direction. In the y direction transmittive boundary conditions were imposed on $n(\partial n/\partial y = 0)$ and Neumann $(\partial\phi_1/\partial y = 0)$ boundary conditions were imposed on ϕ_1.

Three kinds of plots will be presented: (1) contours of constant $n(x,y,t)$; (2) contours of constant $n(x,y,t)/n_o(y,t)$; and (3) contours of constant electrostatic potential ϕ_1. Superimposed on each contour plot is a dashed line depicting $n_o(y,t)$ for reference purposes. Our $n_o(y,o)$ profile is such that the F2 peak is located at 434km altitude, and the minimum electron density scale length $L = n_o(\partial n_o/\partial y)^{-1}$ is 10km. The simulations are all identical except for the east-west grid spacing Δx and the form of the initial perturbation. Two kinds of initial perturbations were used:

Perturbation A:

$$\begin{cases} \dfrac{n(x,y,0)}{n_o(y,0)} = 1 - e^{-3}\cos\left(\dfrac{\pi x}{8\Delta x}\right), & 0 \le |x| \le 8\Delta x \\ \dfrac{n(x,y,0)}{n_o(y,0)} = 1 - e^{-3}\dfrac{1}{2}\left[\cos\left(\dfrac{\pi x}{8\Delta x}\right) - 1\right], & 8\Delta x \le |x| \le 16\Delta x \\ \dfrac{n(x,y,0)}{n_o(y,0)} = 1, & |x| > 16\Delta x \end{cases} \tag{12}$$

Perturbation B:

$$\frac{n(x,y,0)}{n_o(y,0)} = 1 - e^{-3}\cos\left(\frac{\pi x}{20\Delta x}\right) \tag{13}$$

Perturbation A is exactly the form used in Ossakow et al. [1979], and perturbation B is a pure sine wave of wavelength 40 Δx (our system length in the x direction). Both represent maximum initial perturbation amplitudes of approximately 5%. Four simulations have been run: (i) 1S-Perturbation A with Δx = 200m; (ii) 1L-Perturbation A with Δx = 5km; (iii) 2S-Perturbation B with Δx = 200 m; and (iv) 2L-Perturbation B with Δx = 5km. Calculation 1S above is identical to ESF III of Ossakow et al. [1979]. The "large" versus "small" comparison obviously involves comparing calculation 1S to calculation 1L, and calculation 2S to calculation 2L. One notes that for the minimum L $\approx$ 10km in our simulation, kL > 1 for the 1S and 2S cases and kL < 1 for the 1L and 2L cases.

Figure 2 shows isodensity contours of calculation 1S at times 300, 700, 1000, and 1200 seconds after initialization. Figure 3 shows the same contours at the same times but for calculation 1L. The presence of much lower density fluid in the bubble in calculation 1L is obvious. Also obvious is a basic difference in the bubble morphology at late times. At 1200 seconds, 1S has pinched off into two bubbles, with the more intense one below the initial central bubble. In addition, another bubble has formed in the sides of the calculation . These structures are more obvious in the plot of $n(x,y)/n_o(y)$ at 1200 seconds for 1S shown in Fig. 4a. The maximum depletion levels are 70% in the top central bubble,97% in the lower central bubble, and 95% in the side bubble. Note that here and in all subsequent plots of $(n,x,z)/n_o(z)$ the contour plotting is such that the first

(outer) depletion contour n/n_o is 0.5 and each succeeding inner contour is 0.5 times the previous one. For example, the lower bubble in Fig. 4a has five contours. The outermost would have $n/n_o = 0.50$ (50% depletion), the next inner one $n/n_o = 0.25$ (75% depletion), the second inner one $n/n_o = 0.125$ (87.5% depletion) and the innermost $n/n_o = 0.03$ (97% depletion). For the enhancement contours (dashed lines) the first outer contour is 2.0 and the succeeding inner ones are 2.0 times the previous ones. In obtaining percentage enhancements and depletions one then subtracts 1.0.

Calculation 1L, on the other hand, shows a single plume of depleted ionization at 1200 seconds, with no secondary central bubble and no side bubble. There also is no indication of a widening of the top of the bubble, as there is in 1S. In Fig. 4b we show a plot of $n(x,y)/n_o(y)$ for 1L at 1200 sec. The level of depletion is greater than 99.9% for the entire 10km by 70km oval "hole" located inside the tenth solid contour of Fig. 4b and represents at least a three order of magnitude decrease (biteout) in plasma density.

We now repeat the above comparison, but this time for perturbation B (calculations 2S and 2L). Figure 5 shows isodensity contours of calculation 2S at times 300, 700, 1000, and 1091 seconds after initialization; while Figure 6 shows similar plots of calculation 2L at times 700, 1000, 1200 and 1364 sec. Comparison again shows the presence of much lower density plasma in the bubble in the 2L calculation. Morphological differences are also present, the most notable being the widening of the top of the bubble in 2S

which is not present in 2L. Figure 7 shows a comparison of the n/n_o profiles at late time. Again maximum depletions in the 2S case are about 97%, while a large portion of the 2L plume is 99.9% depleted or greater.

We can also compare the effect of the form of the perturbation by comparing 1S to 2S and 1L to 2L. The latter comparison shows striking similarity, whereas the former shows some differences, the most notable being the lack of central bubble "pinching" and the lack of lateral bubbles in case 2S. We conclude that the morphology of the late-time bubbles is dependent, at least somewhat, on the form of the initial perturbation.

Bubble rise velocities are of some interest, and we give below the average bubble rise velocity for each case, computed from the last two frames of Figs. 2, 3, 5, and 6:

1S	210 m/sec
1L	230 m/sec
2S	420 m/sec
2L	280 m/sec

The rise velocity of an individual bubble is dependent upon the relative depletion level of the bubble, its geometry, and upon interactions with other plasma structure nearby. These first two effects are treated in Ossakow and Chaturvedi [1978], and the present results above are consistent with the results therein. For instance, the relatively high

rise velocity associated with 2S is seen to be due to the fact that the bubble is more severely depleted than that in 1S. Further, the roughly equal rise velocities of the 1S, 1L, and 2L bubbles, in spite of the fact that the 1L and 2L bubbles are much more severely depleted than that in 1S, is explained by noting that 1S actually approximates the geometry of a "sheet" of depleted plasma, whereas the 1L and 2L bubbles more closely resemble a cylindrical geometry (see Ossakow and Chaturvedi [1978]).

In an attempt to understand the reasons for the differences in the nonlinear evolution of small and large horizontal scale perturbations, we look at the potential equation:

$$\nabla^2 \phi_1 + \frac{\nabla(\nu_{in}^n)}{\nu_{in}^n} \cdot \nabla \phi_1 = \frac{-Bg}{c\,\nu_{in}} \frac{1}{n} \frac{\partial n}{\partial x}$$

At early times we expect $\nabla \phi_1$ to be small with respect to $Bg/c\nu_{in}$, so we ignore the second term on the left hand side, giving a Poisson equation for ϕ_1:

$$\nabla^2 \phi_1 = - \frac{Bg}{c\nu_{in}} \frac{1}{n} \frac{\partial n}{\partial x}$$

We can now interpret the right hand side as simply the local charge density ρ (such that $\nabla \cdot \underline{E} = \rho$). Since we have initialized all of these calculations with $\frac{1}{n} \frac{\partial n}{\partial x}$ independent of y (see (12)), what we are dealing with is a distribution of charge density that has the form of diffuse "plates" aligned in the vertical direction. Noting that the

term ν_{in} decreases with altitude, we find that these diffuse "plates" have an equally diffuse "edge" in the y direction. Taking the analogy to its conclusion, we model our initial conditions, or any vertically aligned structure for that matter, as an array of plates of charge (non-conducting capacitor plates) with an edge somewhere in or above our grid. In Figure 8 we show schematically the electric potential field surrounding the edge of parallel plates of charge for two different separation distances. Since there is only one scale length in the configuration (the plate separation distance d), then all other scale lengths must be proportional to this distance. In particular, the characteristic distance parallel to the plates over which the electric field outside the plates (the fringe field) falls off must be proportional to d. Since in our problem the contours of electrostatic potential are in fact streamlines (see (11)), this distance will determine the maximum depth in the fluid from which the electrostatic field will draw fluid into the bubble. Since the plasma density is lower at greater depths, this distance will determine the minimum plasma density inside the bubble. To test these ideas, we examine the actual early time electrostatic potential fields from the calculations we have presented. Fig. 9 shows contours of n and ϕ_1 for the 1S initial conditions, and the same plots for 1L. A similar comparison for cases 2S and 2L is shown in Fig. 10. All contour plots of ϕ_1 are scaled in such a way as to evenly space exactly 12 contour lines between the maximum and minimum value of ϕ_1, to normalize the plots so they can be compared without bias. The increased vertical extent of the contours of ϕ_1 (streamlines) for

cases 1L and 2L are evident.

Of course, the initial profile generating these aligned plates of charge lasts only a short time. In the linear phase of growth, the perturbation grows in the region of linear instability (the F region bottomside), and damps elsewhere. Our "plates" therefore very quickly become horizontally spaced regions of charge with a limited vertical extent, confined to the region of steepest vertical gradient on the F region bottomside. Nonetheless, the scaling arguments advanced above still hold: the vertical extent of the polarization electric field scales as the horizontal extent of the structure causing the field. This is easily seen in Figure 11 and 12 where comparison is made of the ϕ_1 contours for 1S vs 1L and 2S vs 2L respectively, at a time of 700 sec. Cases 1S and 2S are seen to be mixing fluid over a fairly narrow altitude range, while 1L and 2L have each formed a large convective cell more than 150km in vertical extent, drawing plasma fluid into the bubble from deep in the ionosphere. It is not surprising, then, that the larger horizontal scale bubbles are more severely depleted at late times.

IV. SUMMARY

On the basis of our numerical simulations, and of a qualitative scale analysis of the driving electrostatic potential equation, we conclude that the severe "biteouts" of three orders of magnitude and bubble rise velocities of 150 m/sec reported by McClure et al [1977] are completely consistent with large ($\sim$75-200km) horizontal bubble

size scales. In our simulations, the severe biteouts associated with large horizontal scale lengths are due to the fact that the plasma comprising these bubbles has its origin at much lower altitudes then in the small horizontal length scale cases. Again, these results are consistent with those of McClure et al. [1977], who base their conclusions on ion mass spectrometer measurements of the $H^+ - O^+ - N^+$ balance inside the bubbles, which they find to be "characteristic of undisturbed plasma found at lower altitudes." The variation in the vertical velocities of various bubbles noted by McClure et al. [1977] is probably due to interactions between bubbles. Note, for example, that in Fig. 2, the secondary bubble is rising at a much slower rate than is the central bubble. Bubble interaction will be the subject of forthcoming theoretical and numerical studies.

APPENDIX: Numerical Solution of the Equations

Of the two partial differential equations we must solve, (10) is elliptic and linear and (11) is hyperbolic and nonlinear. Both equations represent numerical challenges, and we could easily devote the bulk of this paper to the numerical techniques used for their solution. However, as we stated in the introduction, we shall confine ourselves to the improvements made in these techniques since the calculations of Ossakow et al. [1979]. We begin with (11).

Equation (11) is solved in finite difference form using a fully multidimensional second order in time, fourth order in space, leapfrog-trapezoidal flux-corrected transport (FCT) scheme. Both the higher order leapfrog-trapezoidal scheme itself, as well as the fully multidimensional algorithm utilized in the critical flux-limiting stage of FCT, are recent developments and are described by Zalesak [1979]. These developments represent significant extensions of the theory of FCT, a numerical technique originated by Boris and Book [1973] to handle equations of the form (11) where steep gradients are expected for form. By contrast, the calculations in Ossakow et al. [1979] used a first order in time, second order in space FCT algorithm which was only one-dimensional (since fully multidimensional FCT algorithms did not exist at the time), and hence used time-splitting (sequential x and y operators) to solve the two-dimensional equation (11). It is known that time-splitting can introduce numerical

problems into an incompressible flow calculation (see Zalesak, 1979), although our previous equatorial spread F calculations did not exhibit any of the symptoms of these difficulties.

Equation (10) is the elliptic equation whose solution gives us the electrostatic potential ϕ_1. The right hand side is known and the left hand side represents a Hermitian operator operating on ϕ_1, giving only real eigenvalues and apparently easing the difficulty of solution. However, the extremely large range for the values of the quantity $\nu_{in}\, n$ makes for an equally large span of operator eigenvalues, and solution of the equation in this form using iterative techniques has not been successful. We have found one (and only one) method of direct solution, the stabilized error vector propagation (SEVP) method of Madala [1978], but the execution speeds for SEVP are not as favorable as for the method we now describe.

We start by expanding the operator and dividing through by $\nu_{in}\, n$, as was done by Ossakow et al. [1979], giving

$$\nabla_\perp^2 \phi_1 + \frac{\nabla(\nu_{in} n)}{\nu_{in} n} \cdot \nabla_\perp \phi_1 = - \frac{Bg}{c\, \nu_{in}} \frac{1}{n} \frac{\partial n}{\partial x} \qquad \text{(A-1)}$$

The equation is now in a form suitable for solution by the Chebychev-iterative relaxation technique of McDonald [1977]. However, great care must be given to the differencing of the term $\frac{1}{\nu_{in} n} \nabla(\nu_{in} n)$ and $\frac{1}{n} \frac{\partial n}{\partial x}$, and this is the point we wish to address. We work with the term $\frac{1}{n} \frac{\partial n}{\partial x}$ in one spatial dimension, since this example will make the point. A straightforward second-order difference form for this term is

$$\left(\frac{1}{n}\frac{\partial n}{\partial x}\right)_i = \frac{1}{2\Delta x}\ \frac{n_{i+1}-n_{i-1}}{n_i} \qquad \text{(A-2)}$$

where the subscript i refers to grid point location in the x direction and Δx is the (uniform) spacing between grid points. This is the form used in Ossakow et al. [1979]. We shall show that this difference form produces solutions ϕ_1 with potentially undesirable properties, and causes undue numerical hardship in finding those solutions.

Let us rewrite $\frac{1}{n}\ \frac{\partial n}{\partial x}$ as $\frac{\partial}{\partial x}$ (ln n). A physical interpretation of the term is now much easier: the term tells us how rapidly the logarithm of n is varying with respect to x. Suppose, for argument's sake, that the smallest and largest values of n in the problem are 10^1 and 10^5 respectively. On a grid of size Δx, the largest value representable for that term would occur when a fluid element of density 10^1 and one of density 10^5 occupy adjacent grid points. The value of $\frac{\partial}{\partial x}$ (ln n) evaluated midway between these two grid points would be $\frac{1}{\Delta x}$ (ln 10^5 - ln 10^1) = 9.2 Δx^{-1}. Evaluation of (A-2) for n_{i-1},n_i, and n_{i+1} having values of 10^1, 10^1, and 10^5 respectively gives a value for $\left(\frac{1}{n}\ \frac{\partial n}{\partial x}\right)_i$ of 5 x 10^4 Δx^{-1}, far in excess of the maximum value for this term given by the above argument. Logarithmic interpretation of this term would state that n varied by more than 10^4 orders of magnitude over a single grid spacing, a ridiculous statement in light of the fact that there are only four orders of magnitude of n in the problem.

The potentially large values of these terms, in particular of the term $\frac{1}{\nu_{in} n} \nabla_\perp (\nu_{in} n)$ in (A-1), not only cause extremely slow convergence of the iterative solution, but can also put **spurious** oscillations into the exact finite difference solution ϕ_1 due to cell Reynolds number effects [Roache, 1976]. As shown by Roache [1976] these oscillations can occur any time the value of the term $\frac{1}{\nu_{in} n} \nabla_\perp (\nu_{in} n)$ in (A-1) exceeds a critical value of $2 \Delta x^{-1}$. It is clear, then, that (A-2) represents an undesirable difference form for these logarithmic terms. Better approximations are

$$\left(\frac{1}{n} \frac{\partial n}{\partial z}\right)_i = \frac{1}{2\Delta x} (\ln n_{i+1} - \ln n_{i-1}) \qquad \text{(A-3)}$$

and

$$\left(\frac{1}{n} \frac{\partial n}{\partial x}\right)_i = \frac{1}{\Delta x} \frac{n_{i+1} - n_{i-1}}{n_{i+1} + n_{i-1}} \qquad \text{(A-4)}$$

Equation (A-3) is probably the most accurate, but evaluation of the logarithms at every time step is computationally expensive, and for problems like the one at hand where n varies by many orders of magnitude across the grid, there is still no guarantee that the critical cell Reynolds number will not be exceeded. For these reasons we use (A-4) for the present calculations.

Acknowledgement

This work was supported by the Defense Nuclear Agency and the Office of Naval Research.

References

Booker, H. G., The role of acoustic gravity waves in the generation of spread-F and ionospheric scintillation, J. Atmos. Terr. Phys., 41, 501, 1979.

Boris, J. P., and D. L. Book, Flux-corrected transport, I, Shasta, a transport algorithm that works, J. Comp. Phys., 11, 38, 1973.

Klostermeyer, J., Nonlinear investigation of the spatial resonance effect in the nighttime equatorial F region, J. Geophys. Res., 83, 3753, 1978.

Madala, R. V., An efficient direct solver for separable and non-separable elliptic equations, Monthly Weather Rev., 106, 1735, 1978.

McClure, J. P., W. B. Hanson, and J. H. Hoffman, Plasma bubbles and irregularities in the equatorial ionosphere, J. Geophys. Res., 82, 2650, 1977.

McDonald, B. E., Explicit Chebychev-iterative solution of nonself-adjoint elliptic equations on a vector computer NRL Memo Rep. 3541, Nav. Res. Lab., Washington, D. C., June, 1977.

Ossakow, S. L. and Chaturvedi, P. K., Morphological studies of rising equatorial spread F bubbles, J. Geophys. Res., 83, 2085, 1978.

Ossakow, S. L., S. T. Zalesak, B. E. McDonald, and P. K. Chaturvedi, Nonlinear equatorial spread F: Dependence on altitude of the F peak and bottomside background electron density gradient scale length, J. Geophys. Res., 84, 17, 1979.

Roache, P.J., Computational Fluid Dynamics, Hermosa Publishers, Albuquerque, N. M., 1976

Rottger, J., The macro-scale structure of equatorial spread-F irregularities, J. Atmos. Terr. Phys., 38, 97, 1976.

Scannapieco, A. J., and S. L. Ossakow, Nonlinear equatorial spread-F, Geophys. Res. Lett., 3, 451, 1976.

Zalesak , S. T., Fully multidimensional flux-corrected transport algorithms for fluids, J. Comput. Phys., 31, 335, 1979.

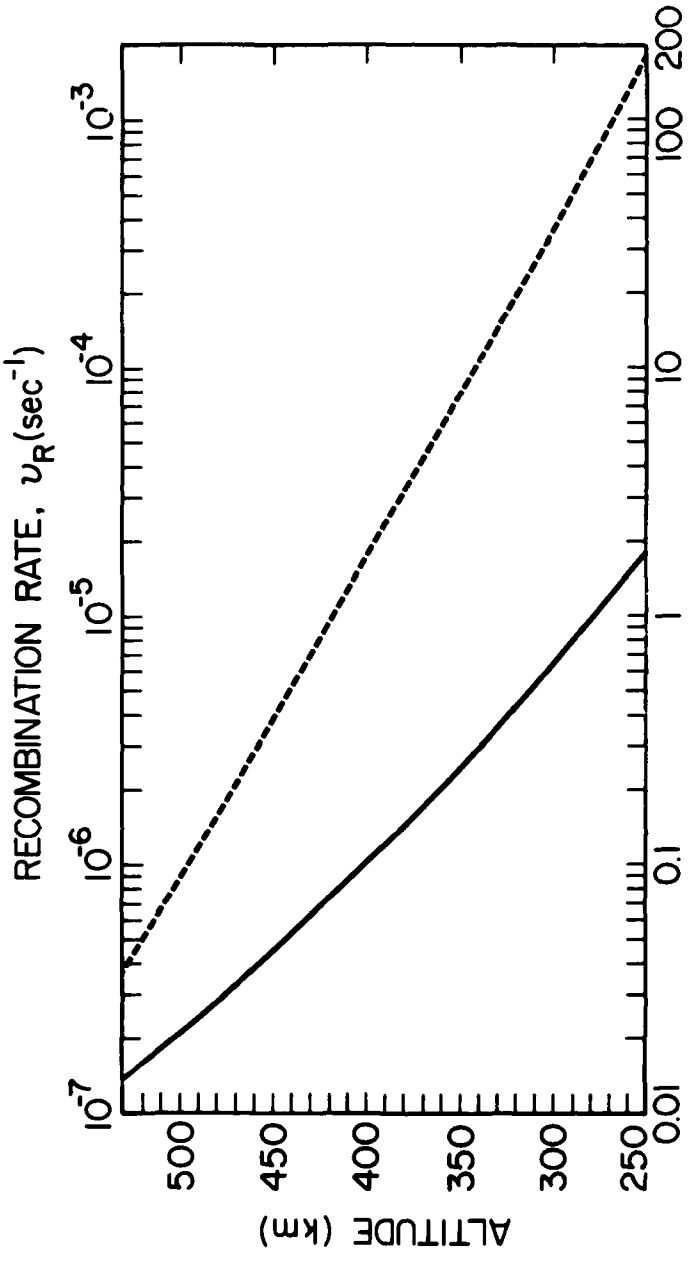

Fig. 1 - The ion-neutral collision frequency ν_{in} and recombination rate ν_R (as a function of altitude) used in the numerical simulations

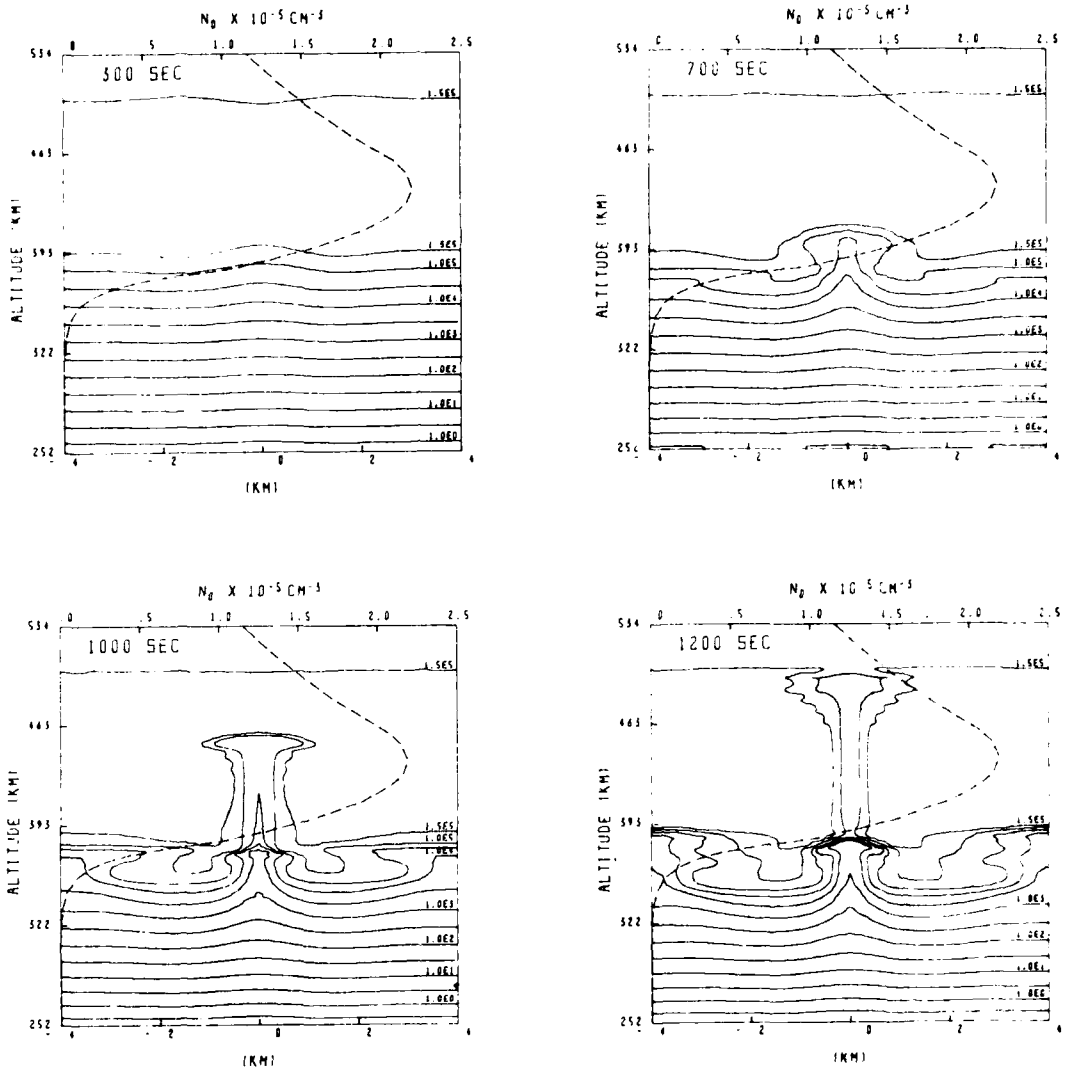

Fig. 2 - Sequence of four plots showing iso-electron density contours of calculation 1S at 300, 700, 1000, and 1200 sec. Superimposed on each plot is a dashed line depicting $n_o(z,t)$. Electron densities are given in cm^{-3}. The observer is looking southward.

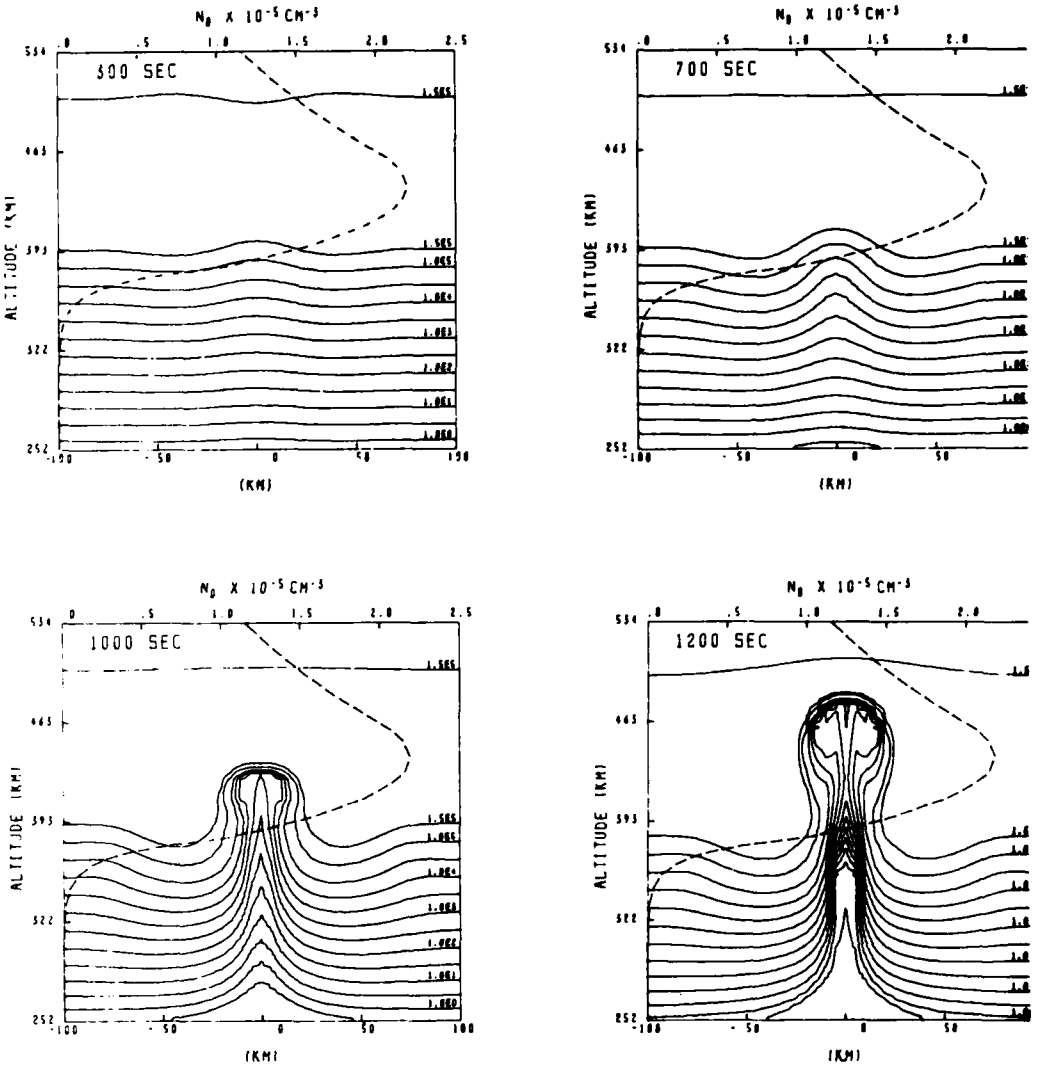

Fig. 3 - Same as Fig. 2 but for calculation 1L

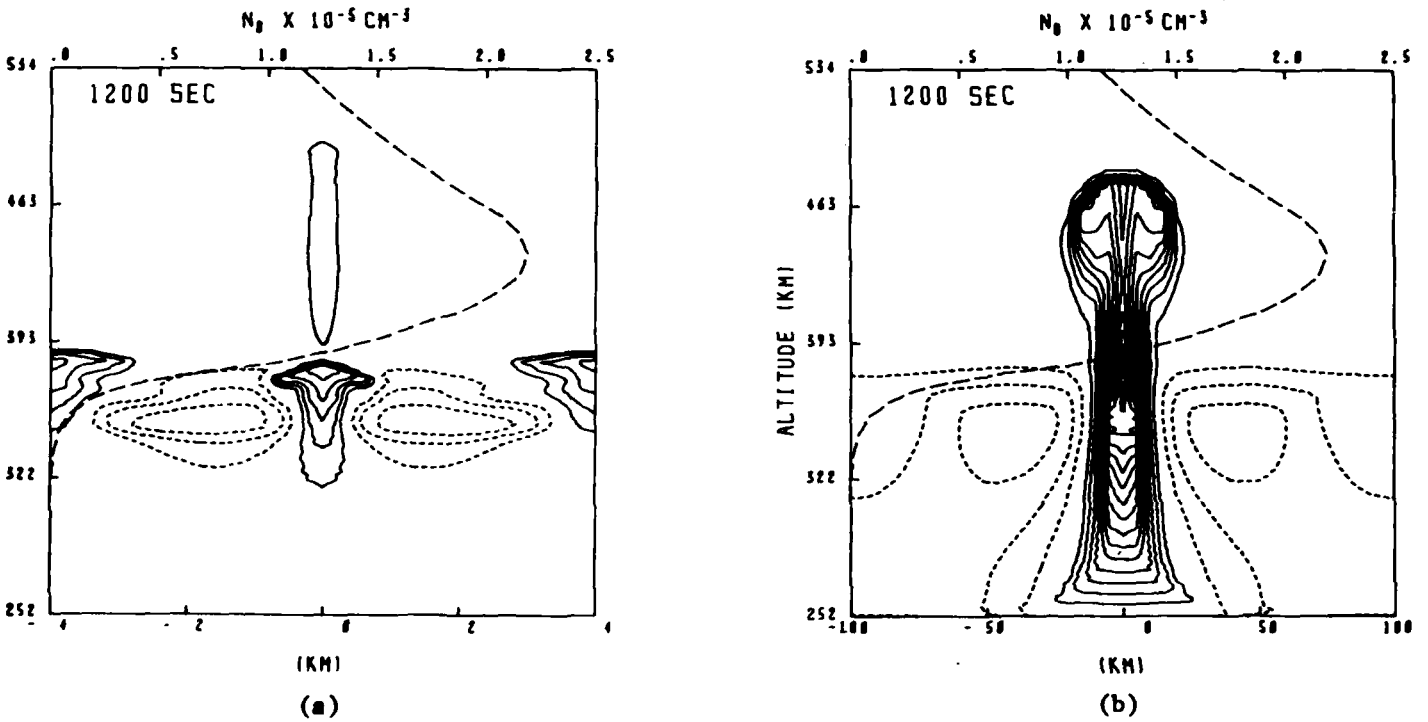

Fig. 4 - Contours of constant $n(x,y,t)/n_o(z,t)$ for a) 1S at 1200 sec and b) 1L at 1200 sec. Depletions ($n/n_o < 1$) are shown in solid lines while enhancements ($n/n_o > 1$) are shown as short dashed lines. The first (outermost) depletion contour is for $n/n_o = 0.5$, while each suceeding contour is for a value of n/n_o a factor of 0.5 times the previous one. The first enhancement contour is for $n/n_o = 2.0$, while each suceeding contour is for a value of n/n_o a factor of 2.0 times the previous one. The superimposed long dashed line depicts $n_o(z,t)$.

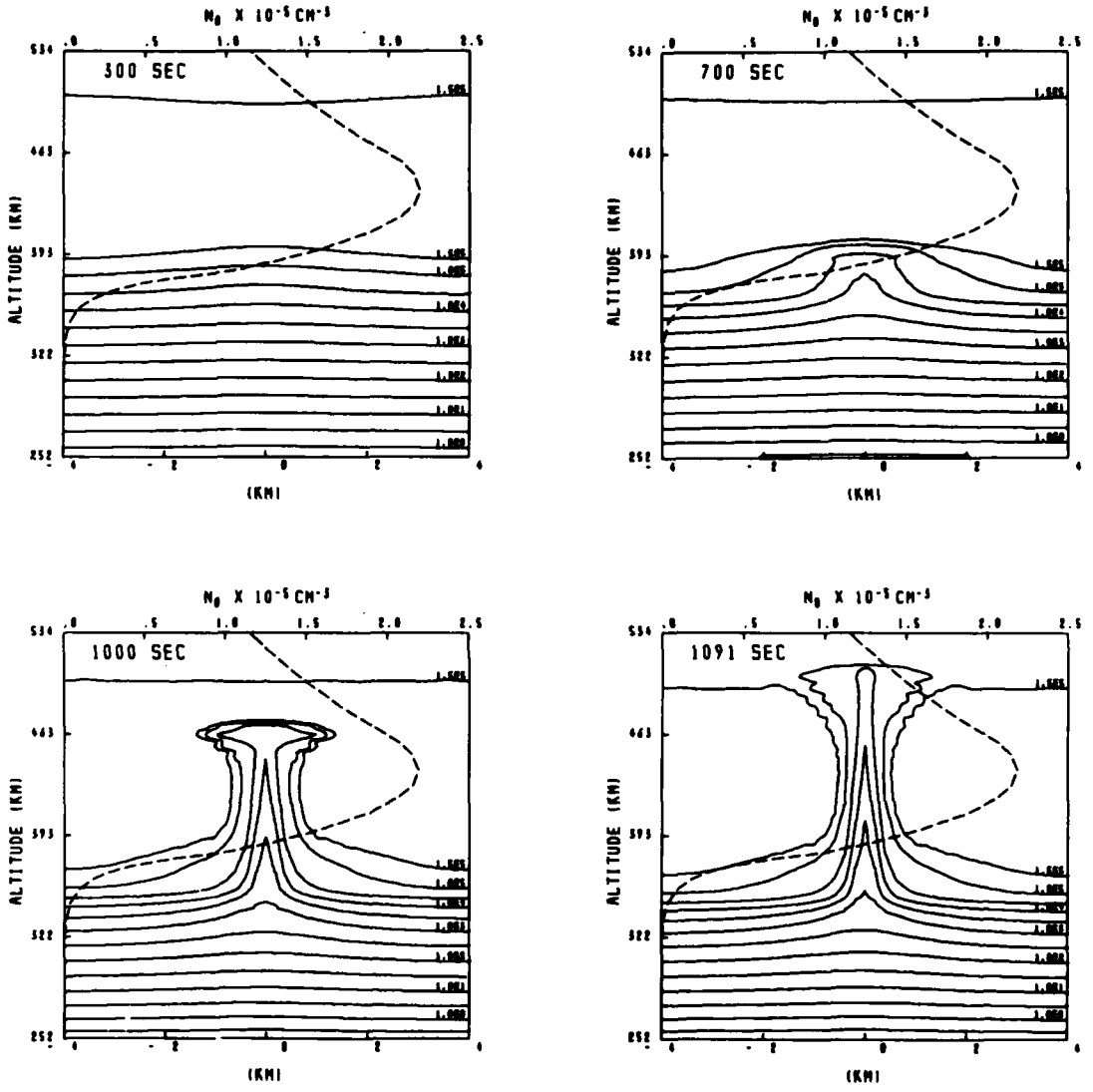

Fig. 5 - Same as Fig. 2 but for calculation 2S at 300, 700, 1000, and 1091 sec.

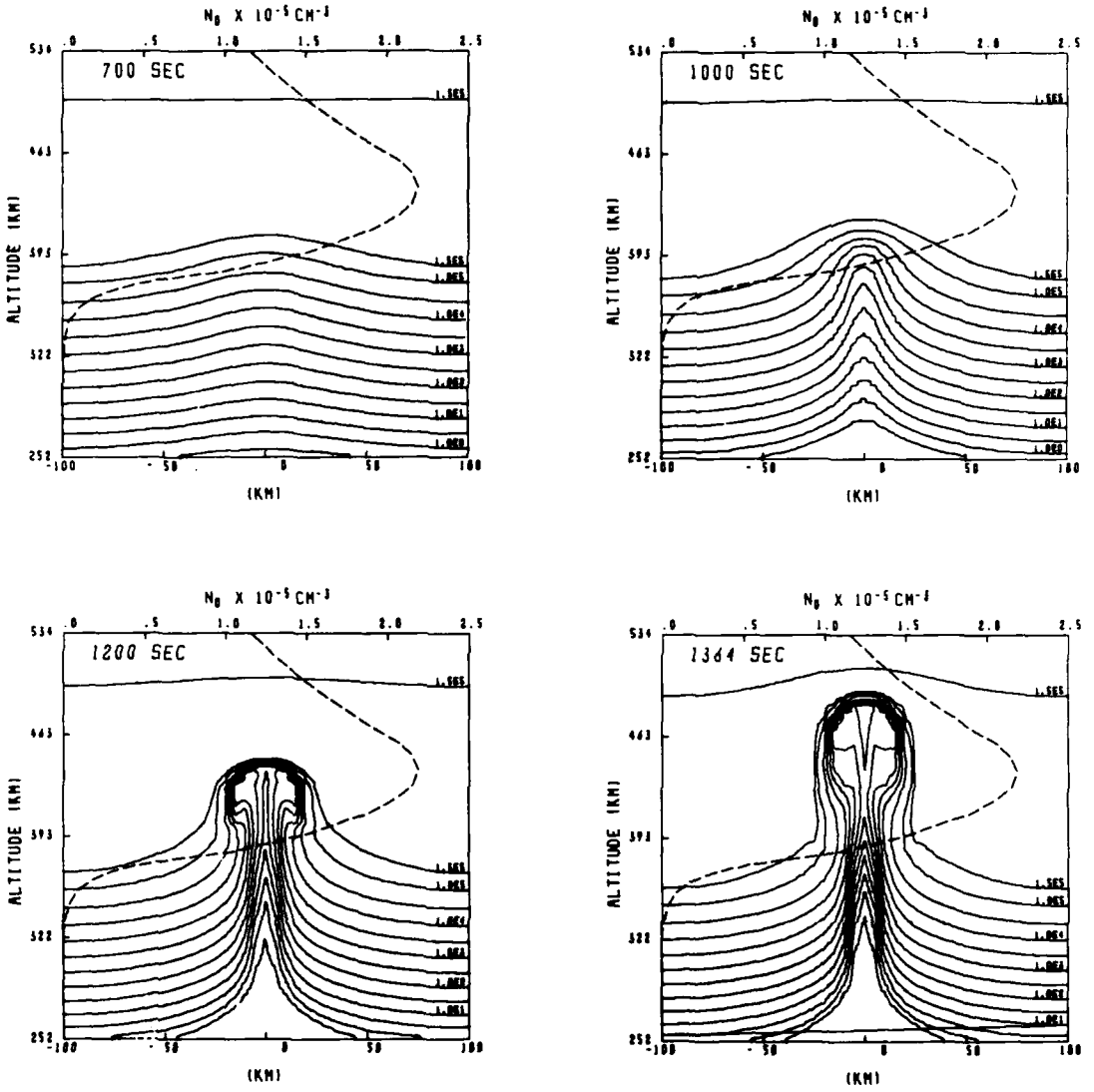

Fig. 6 - Same as Fig. 5 but for calculation 2L at 700, 1000, 1200, and 1364 sec.

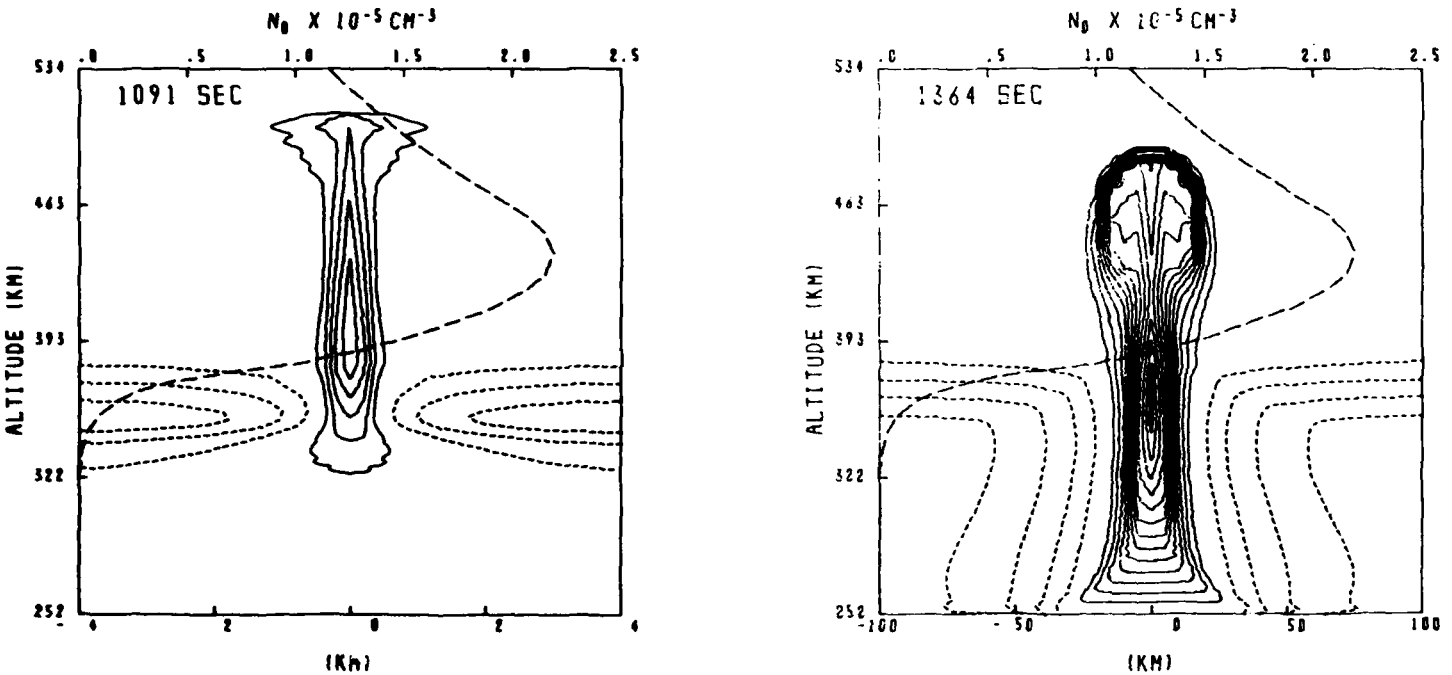

Fig. 7 - Same as Fig. 4 but for a) calculation 2S at 1091 sec and b) calculation 2L at 1364 sec.

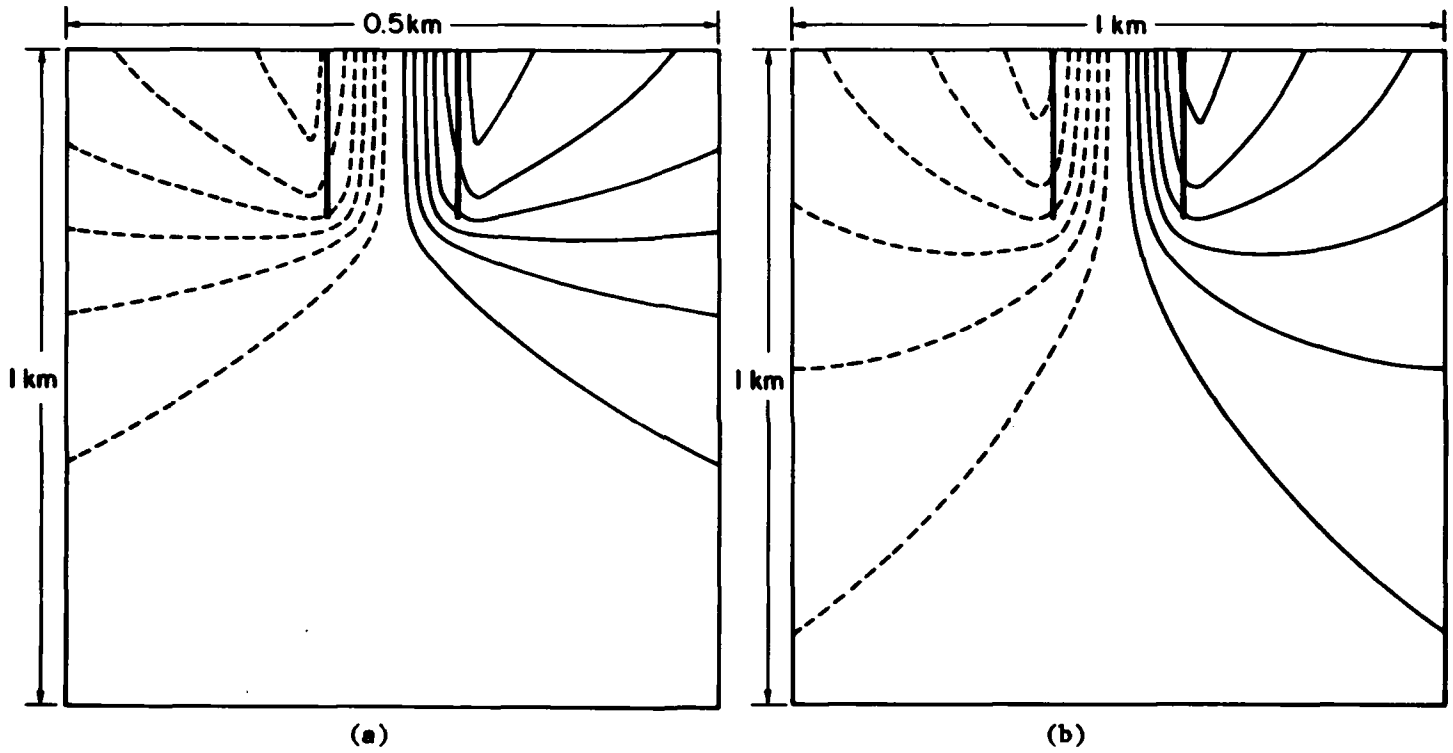

Fig. 8 - Schematic representation of contours of constant electrostatic potential produced at the edge of non-conducting parallel plates of charge for two different plate separation distances: a) 0.5 km and b) 1.0 km. Dashed lines are for negative potentials and solid lines are for positive potentials. The potential drop across adjacent contours is a constant in each plot, except that the zero potential (which would just be a vertical line) is not plotted. In each case the contours are chosen to space the twelve contours (plus the zero contour) uniformly from maximum to minimum potential. Since the electric field magnitude is inversely proportional to the contour spacing, we have, in effect, normalized each plot to the maximum electric field found between the plates. This facilitates the comparison of the rate at which the electric field falls off away from the edge of the plates. The much more rapid falloff in a) is evident.

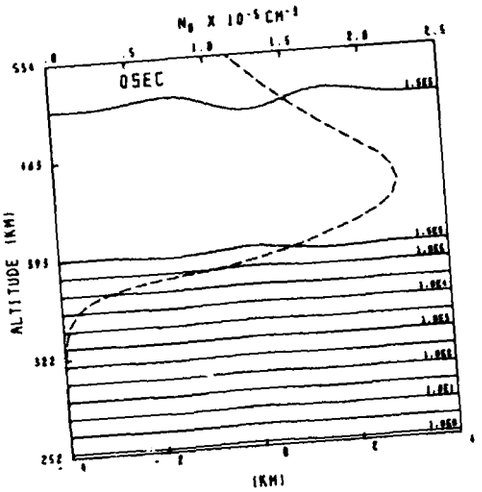

Figure 9(a)

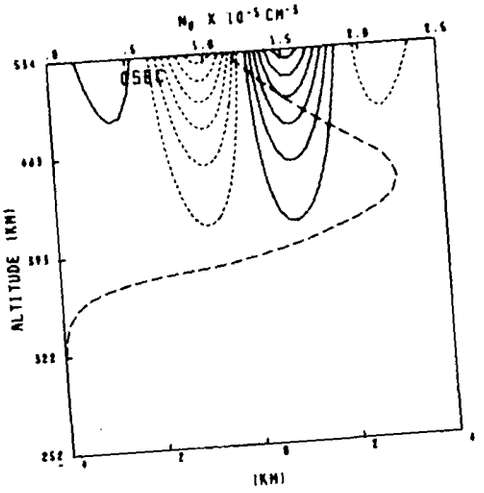

Figure 9(b)

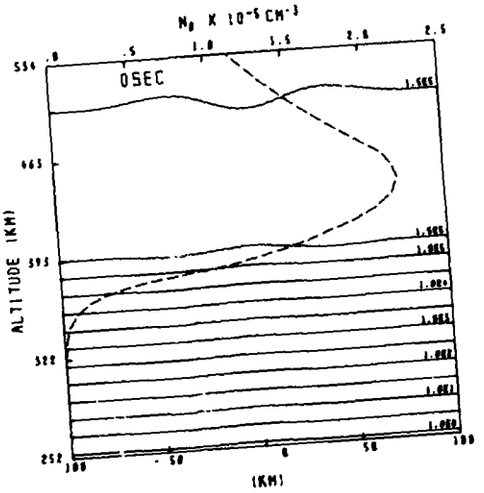

Figure 9(c)

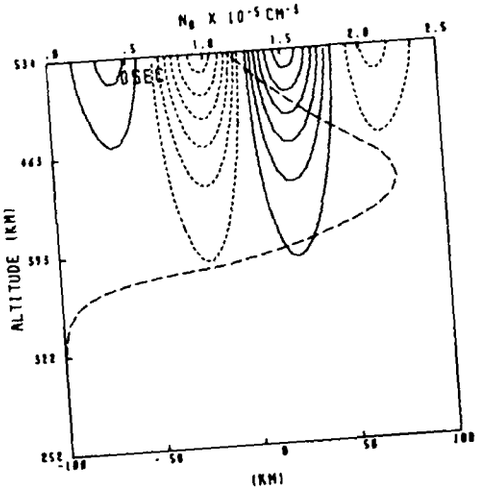

Figure 9(d)

Fig. 9 - Iso-electron density plots at t = 0 for 1S (a) and 1L(c). Also shown are the corresponding contours of constant induced electrostatic potential in (b) and (d) respectively. For the plots of electrostatic potential, the comments from Fig. 8 apply. Since the contours of constant potential are in fact flow streamlines, more plasma from lower altitudes is being drawn upward in the 1L case than in the 1S case.

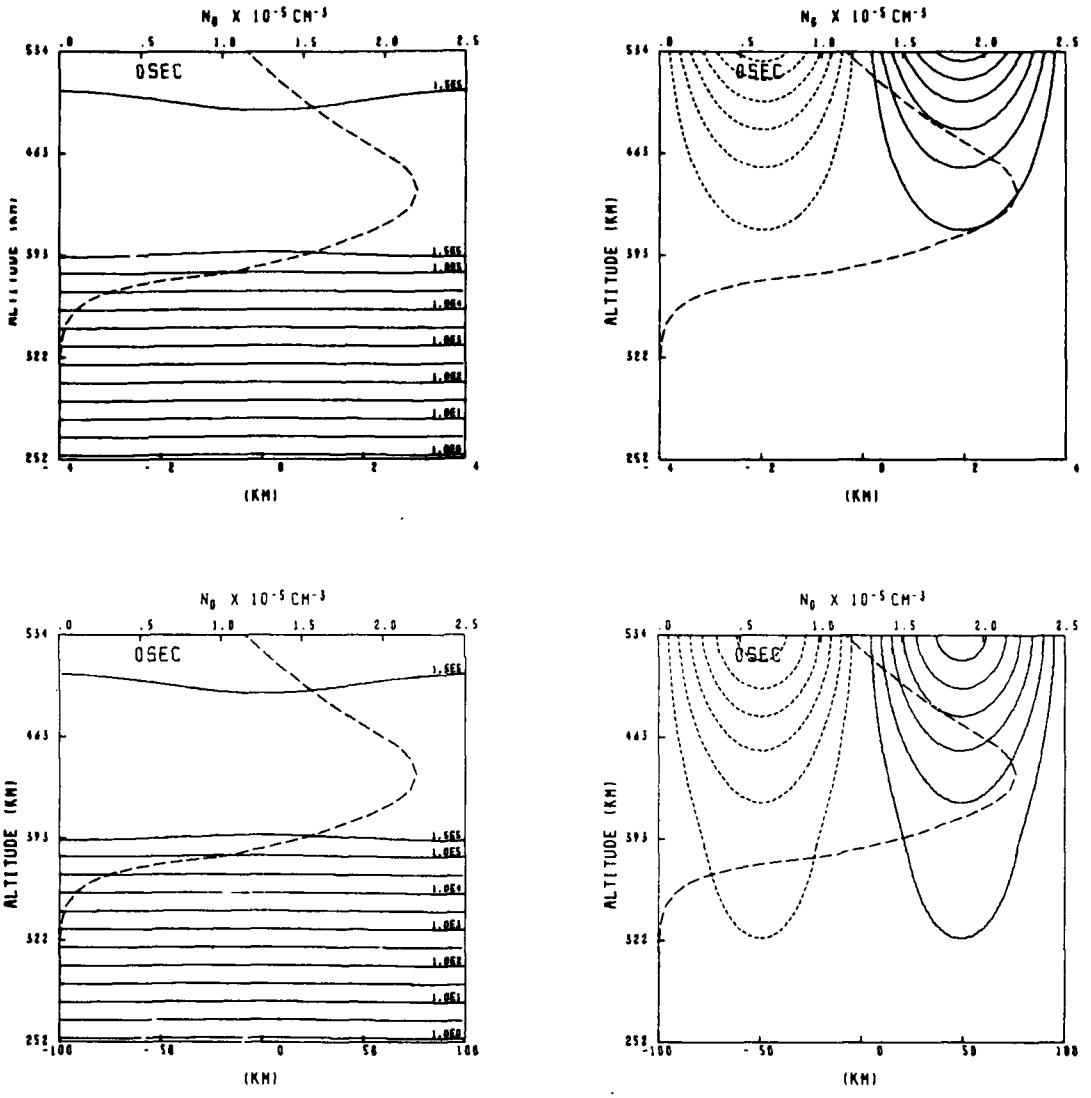

Fig. 10 - Same as Fig. 9 but for cases 2S and 2L

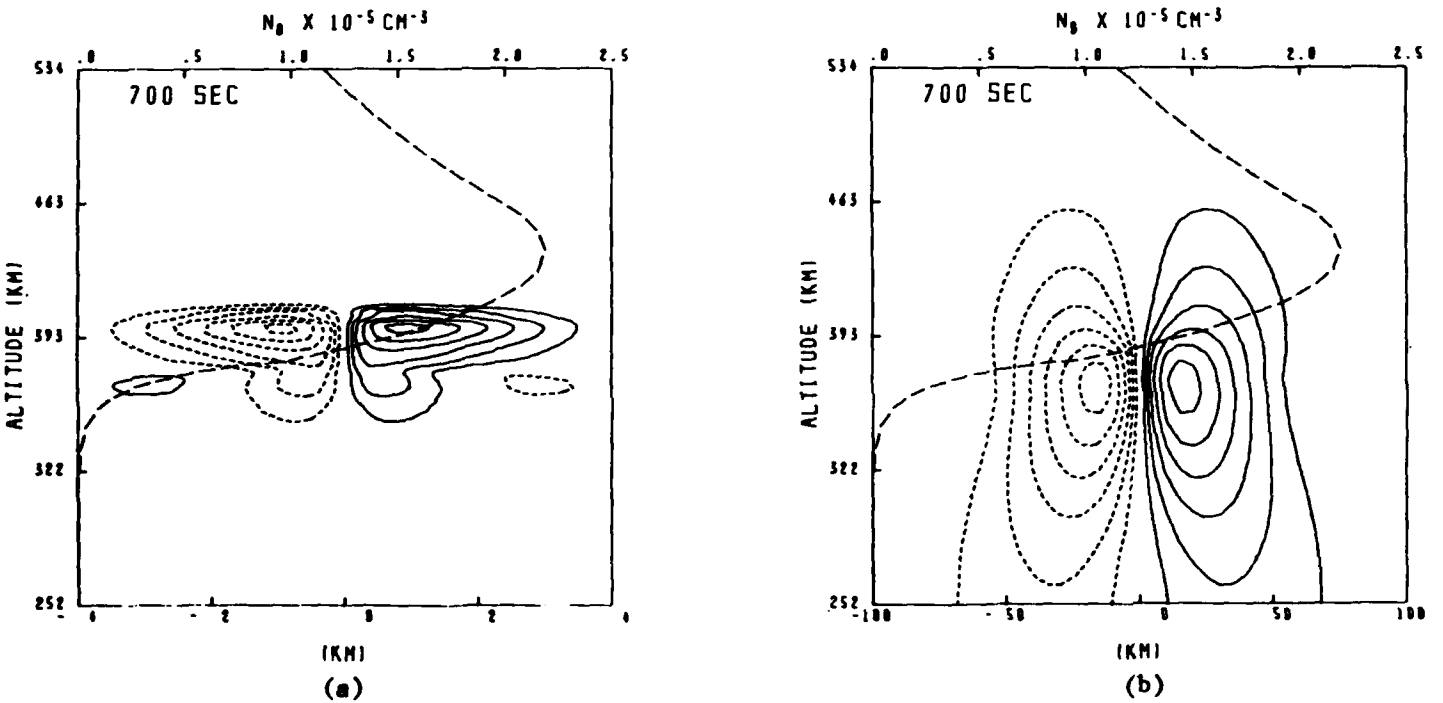

Fig. 11 - Contours of constant electrostatic potential at 700 sec for (a) calculation 1S and (b) calculation 1L. Comments from Fig. 8 and Fig. 9 apply.

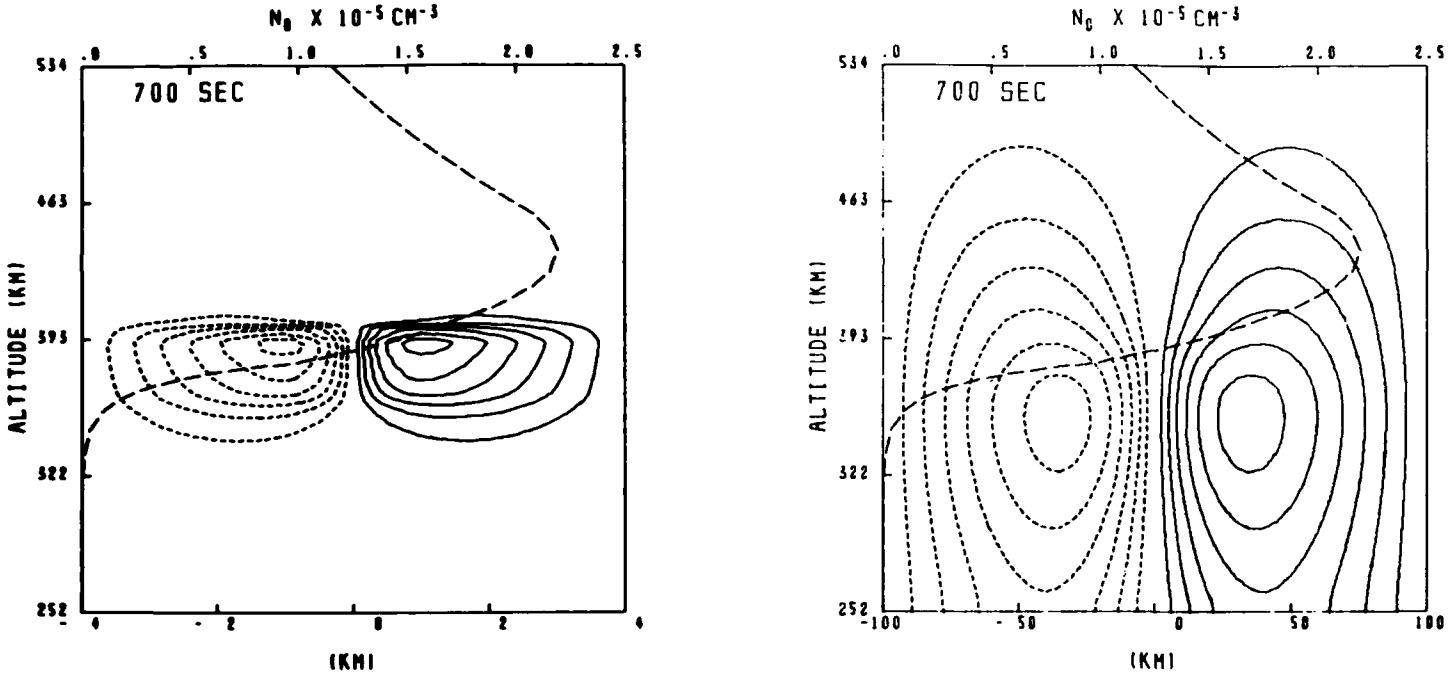

Fig. 12 - Same as Fig. 11 but for (a) calculation 2S and (b) calculation 2L.

DISTRIBUTION LIST

DEPARTMENT OF DEFENSE

ASSISTANT SECRETARY OF DEFENSE
COMM, CMD, CONT & INTELL
WASHINGTON, D.C. 20301
01CY ATTN J. BABCOCK
01CY ATTN M. EPSTEIN

ASSISTANT TO THE SECRETARY OF DEFENSE
ATOMIC ENERGY
WASHINGTON, D.C. 20301
01CY ATTN EXECUTIVE ASSISTANT

DIRECTOR
COMMAND CONTROL TECHNICAL CENTER
PENTAGON RM BE 685
WASHINGTON, D.C. 20301
01CY ATTN C-650
01CY ATTN C-312 R. MASON

DIRECTOR
DEFENSE ADVANCED RSCH PROJ AGENCY
ARCHITECT BUILDING
1400 WILSON BLVD.
ARLINGTON, VA. 22209
01CY ATTN NUCLEAR MONITORING RESEARCH
01CY ATTN STRATEGIC TECH OFFICE

DEFENSE COMMUNICATION ENGINEER CENTER
1860 WIEHLE AVENUE
RESTON, VA. 22090
01CY ATTN CODE R820
01CY ATTN CODE R410 JAMES W. MCLEAN
01CY ATTN CODE R720 J. WORTHINGTON

DIRECTOR
DEFENSE COMMUNICATIONS AGENCY
WASHINGTON, D.C. 20305
(ADR CNWDI: ATTN CODE 240 FOR)

01CY ATTN CODE 1018

DEFENSE DOCUMENTATION CENTER
CAMERON STATION
ALEXANDRIA, VA. 22314
(12 COPIES IF OPEN PUBLICATION, OTHERWISE 2 COPIES)
12CY ATTN TC

DIRECTOR
DEFENSE INTELLIGENCE AGENCY
WASHINGTON, D.C. 20301
01CY ATTN DT-1B
01CY ATTN DB-4C E. O'FARRELL
01CY ATTN DIAAP A. WISE
01CY ATTN DIAST-5
01CY ATTN DT-1BZ R. HORTON
01CY ATTN HQ-TR J. STEWART
01CY ATTN W. WITTIG DC-7D

DIRECTOR
DEFENSE NUCLEAR AGENCY
WASHINGTON, D.C. 20305
01CY ATTN STVL
04CY ATTN TITL
01CY ATTN DDST
03CY ATTN RAAE

COMMANDER
FIELD COMMAND
DEFENSE NUCLEAR AGENCY
KIRTLAND AFB, NM 87115
01CY ATTN FCPR

DIRECTOR
INTERSERVICE NUCLEAR WEAPONS SCHOOL
KIRTLAND AFB, NM 87115
01CY ATTN DOCUMENT CONTROL

JOINT CHIEFS OF STAFF
WASHINGTON, D.C. 20301
01CY ATTN J-3 WWMCCS EVALUATION OFFICE

DIRECTOR
JOINT STRAT TGT PLANNING STAFF
OFFUTT AFB
OMAHA, NB 68113
01CY ATTN JLTW-2
01CY ATTN JPST G. GOETZ

CHIEF
LIVERMORE DIVISION FLD COMMAND DNA
DEPARTMENT OF DEFENSE
LAWRENCE LIVERMORE LABORATORY
P. O. BOX 808
LIVERMORE, CA 94550
01CY ATTN FCPRL

DIRECTOR
NATIONAL SECURITY AGENCY
DEPARTMENT OF DEFENSE
FT. GEORGE G. MEADE, MD 20755
01CY ATTN JOHN SKILLMAN R52
01CY ATTN FRANK LEONARD
01CY ATTN W14 PAT CLARK
01CY ATTN OLIVER H. BARTLETT W32
01CY ATTN R5

COMMANDANT
NATO SCHOOL (SHAPE)
APO NEW YORK 09172
01CY ATTN U.S. DOCUMENTS OFFICER

UNDER SECY OF DEF FOR RSCH & ENGRG
DEPARTMENT OF DEFENSE
WASHINGTON, D.C. 20301
01CY ATTN STRATEGIC & SPACE SYSTEMS (OS)

WWMCCS SYSTEM ENGINEERING ORG
WASHINGTON, D.C. 20305
01CY ATTN R. CRAWFORD

COMMANDER/DIRECTOR
ATMOSPHERIC SCIENCES LABORATORY
U.S. ARMY ELECTRONICS COMMAND
WHITE SANDS MISSILE RANGE, NM 88002
01CY ATTN DELAS-EO F. NILES

DIRECTOR
BMD ADVANCED TECH CTR
HUNTSVILLE OFFICE
P. O. BOX 1500
HUNTSVILLE, AL 35807
01CY ATTN ATC-T MELVIN T. CAPPS
01CY ATTN ATC-O W. DAVIES
01CY ATTN ATC-R DON RUSS

PROGRAM MANAGER
BMD PROGRAM OFFICE
5001 EISENHOWER AVENUE
ALEXANDRIA, VA 22333
01CY ATTN DACS-BMT J. SHEA

CHIEF C-E SERVICES DIVISION
U.S. ARMY COMMUNICATIONS CMD
PENTAGON RM 1B269
WASHINGTON, D.C. 20310
01CY ATTN C-E-SERVICES DIVISION

COMMANDER
FRADCOM TECHNICAL SUPPORT ACTIVITY
DEPARTMENT OF THE ARMY
FORT MONMOUTH, N.J. 07703
01CY ATTN DRSEL-NL-RD H. BENNET
01CY ATTN DRSEL-PL-ENV H. BOMKE
01CY ATTN J. E. QUIGLEY

COMMANDER
HARRY DIAMOND LABORATORIES
DEPARTMENT OF THE ARMY
2800 POWDER MILL ROAD
ADELPHI, MD 20783
(CNWDI-INNER ENVELOPE: ATTN: DELHD-RBH)
01CY ATTN DELHD-TI M. WEINER
01CY ATTN DELHD-RB R. WILLIAMS
01CY ATTN DELHD-NP F. WIMENITZ
01CY ATTN DELHD-NP C. MOAZED

COMMANDER
U.S. ARMY COMM-ELEC ENGRG INSTAL AGY
FT. HUACHUCA, AZ 85613
01CY ATTN CCC-EMEO GEORGE LANE

COMMANDER
U.S. ARMY FOREIGN SCIENCE & TECH CTR
220 7TH STREET, NE
CHARLOTTESVILLE, VA 22901
01CY ATTN DRXST-SD
01CY ATTN R. JONES

COMMANDER
U.S. ARMY MATERIEL DEV & READINESS CMD
5001 EISENHOWER AVENUE
ALEXANDRIA, VA 22333
01CY ATTN DRCLDC J. A. BENDER

COMMANDER
U.S. ARMY NUCLEAR AND CHEMICAL AGENCY
7500 BACKLICK ROAD
BLDG 2073
SPRINGFIELD, VA 22150
01CY ATTN LIBRARY

DIRECTOR
U.S. ARMY BALLISTIC RESEARCH LABS
ABERDEEN PROVING GROUND, MD 21005
01CY ATTN TECH LIB EDWARD BAICY

COMMANDER
U.S. ARMY SATCOM AGENCY
FT. MONMOUTH, NJ 07703
01CY ATTN DOCUMENT CONTROL

COMMANDER
U.S. ARMY MISSILE INTELLIGENCE AGENCY
REDSTONE ARSENAL, AL 35809
01CY ATTN JIM GAMBLE

DIRECTOR
U.S. ARMY TRADOC SYSTEMS ANALYSIS ACTIVITY
WHITE SANDS MISSILE RANGE, NM 88002
01CY ATTN ATAA-SA
01CY ATTN TCC/F. PAYAN JR.
01CY ATTN ATAA-TAC LTC J. MESSE

COMMANDER
NAVAL ELECTRONIC SYSTEMS COMMAND
WASHINGTON, D.C. 20360
01CY ATTN NAVALEX 034 T. HUGHES
01CY ATTN PME 117
01CY ATTN PME 117-T
01CY ATTN CODE 5011

COMMANDING OFFICER
NAVAL INTELLIGENCE SUPPORT CTR
4301 SUITLAND ROAD, BLDG. 5
WASHINGTON, D.C. 20390
01CY ATTN MR. DUBBIN STIC 12
01CY ATTN NISC-50
01CY ATTN CODE 5404 J. GALET

COMMANDER
NAVAL SURFACE WEAPONS CENTER
DAHLGREN LABORATORY
DAHLGREN, VA 22448
01CY ATTN CODE DF-14 R. BUTLER

COMMANDING OFFICER
NAVY SPACE SYSTEMS ACTIVITY
P.O. BOX 92960
WORLDWAY POSTAL CENTER
LOS ANGELES, CA. 90009
01CY ATTN CODE 52

OFFICE OF NAVAL RESEARCH
ARLINGTON, VA 22217
01CY ATTN CODE 465
01CY ATTN CODE 461
01CY ATTN CODE 402
01CY ATTN CODE 420
01CY ATTN CODE 421

COMMANDER
AEROSPACE DEFENSE COMMAND/DC
DEPARTMENT OF THE AIR FORCE
ENT AFB, CO 80912
01CY ATTN DC MR. LONG

COMMANDER
AEROSPACE DEFENSE COMMAND/XPD
DEPARTMENT OF THE AIR FORCE
ENT AFB, CO 80912
01CY ATTN XPDQQ
01CY ATTN XP

AIR FORCE GEOPHYSICS LABORATORY
HANSCOM AFB, MA 01731
01CY ATTN OPR HAROLD GARDNER
01CY ATTN OPR-1 JAMES C. ULWICK
01CY ATTN LKB KENNETH S. W. CHAMPION
01CY ATTN OPR ALVA T. STAIR
01CY ATTN PHP JULES AARONS
01CY ATTN PHD JURGEN BUCHAU
01CY ATTN PHD JOHN P. MULLEN

AF WEAPONS LABORATORY
KIRTLAND AFB, NM 87117
01CY ATTN SUL
01CY ATTN CA ARTHUR H. GUENTHER
01CY ATTN DYC CAPT J. BARRY
01CY ATTN DYC JOHN M. KAMM
01CY ATTN DYT CAPT MARK A. FRY
01CY ATTN DES MAJ GARY GANONG
01CY ATTN DYC J. JANNI

AFTAC
PATRICK AFB, FL 32925
01CY ATTN TF/MAJ WILEY
01CY ATTN TN

AIR FORCE AVIONICS LABORATORY
WRIGHT-PATTERSON AFB, OH 45433
01CY ATTN AAD WADE HUNT
01CY ATTN AAD ALLEN JOHNSON

DEPUTY CHIEF OF STAFF
RESEARCH, DEVELOPMENT, & ACQ
DEPARTMENT OF THE AIR FORCE
WASHINGTON, D.C. 20330
01CY ATTN AFRDQ

HEADQUARTERS
ELECTRONIC SYSTEMS DIVISION/XR
DEPARTMENT OF THE AIR FORCE
HANSCOM AFB, MA 01731
01CY ATTN XR J. DEAS

HEADQUARTERS
ELECTRONIC SYSTEMS DIVISION/YSEA
DEPARTMENT OF THE AIR FORCE
HANSCOM AFB, MA 01731
01CY ATTN YSEA

COMMANDER
NAVAL OCEAN SYSTEMS CENTER
SAN DIEGO, CA 92152
03CY ATTN CODE 532 W. MOLER
01CY ATTN CODE 0230 C. BAGGETT
01CY ATTN CODE 81 R. EASTMAN

DIRECTOR
NAVAL RESEARCH LABORATORY
WASHINGTON, D.C. 20375
01CY ATTN CODE 6700 TIMOTHY P. COFFEY
(25 CYS IF UNCLASS, 1 CY IF CLASS)
01CY ATTN CODE 6701 JACK D. BROWN
01CY ATTN CODE 6780 BRANCH HEAD (150 CYS
IF UNCLASS, 1 CY IF CLASS)
01CY ATTN CODE 7500 HQ COMM DIR BRUCE WALD
01CY ATTN CODE 7550 J. DAVIS
01CY ATTN CODE 7580
01CY ATTN CODE 7551
01CY ATTN CODE 7555
01CY ATTN CODE 6730 E. MCLEAN
01CY ATTN CODE 7127 C. JOHNSON

COMMANDER
NAVAL SEA SYSTEMS COMMAND
WASHINGTON, D.C. 20362
01CY ATTN CAPT R. PITKIN

COMMANDER
NAVAL SPACE SURVEILLANCE SYSTEM
DAHLGREN, VA 22448
01CY ATTN CAPT J. H. BURTON

OFFICER-IN-CHARGE
NAVAL SURFACE WEAPONS CENTER
WHITE OAK, SILVER SPRING, MD 20910
01CY ATTN CODE F31

DIRECTOR
STRATEGIC SYSTEMS PROJECT OFFICE
DEPARTMENT OF THE NAVY
WASHINGTON, D.C. 20376
01CY ATTN NSP-2141
01CY ATTN NSSP-2722 FRED WIMBERLY

NAVAL SPACE SYSTEM ACTIVITY
P. O. BOX 92960
WORLDWAY POSTAL CENTER
LOS ANGELES, CALIF. 90009
01CY ATTN A. B. HAZZARD

HEADQUARTERS
ELECTRONIC SYSTEMS DIVISION/DC
DEPARTMENT OF THE AIR FORCE
HANSCOM AFB, MA 01731
01CY ATTN DCKC MAJ J. C. CLARK

COMMANDER
FOREIGN TECHNOLOGY DIVISION, AFSC
WRIGHT-PATTERSON AFB, OH 45433
01CY ATTN NICD LIBRARY
01CY ATTN ETDP B. BALLARD

COMMANDER
ROME AIR DEVELOPMENT CENTER, AFSC
GRIFFISS AFB, NY 13441
01CY ATTN DOC LIBRARY/TSLD
01CY ATTN OCSE V. COYNE

SAMSO/SZ
POST OFFICE BOX 92960
WORLDWAY POSTAL CENTER
LOS ANGELES, CA 90009
(SPACE DEFENSE SYSTEMS)
01CY ATTN SZJ

STRATEGIC AIR COMMAND/XPFS
OFFUTT AFB, NB 68113
01CY ATTN XPFS MAJ B. STEPHAN
01CY ATTN ADWATE MAJ BRUCE BAUER
01CY ATTN NRT
01CY ATTN DOK CHIEF SCIENTIST

SAMSO/YA
P. O. BOX 92960
WORLDWAY POSTAL CENTER
LOS ANGELES, CA 90009
01CY ATTN YAT CAPT L. BLACKWELDER

SAMSO/SK
P. O. BOX 92960
WORLDWAY POSTAL CENTER
LOS ANGELES, CA 90009
01CY ATTN SKA (SPACE COMM SYSTEMS) M. CLAVIN

SAMSO/MN
NORTON AFB, CA 92409
(MINUTEMAN)
01CY ATTN MNNL LTC KENNEDY

COMMANDER
ROME AIR DEVELOPMENT CENTER, AFSC
HANSCOM AFB, MA 01731
01CY ATTN EEP A. LORENTZEN

DEPARTMENT OF ENERGY

DEPARTMENT OF ENERGY
ALBUQUERQUE OPERATIONS OFFICE
P. O. BOX 5400
ALBUQUERQUE, NM 87115
01CY ATTN DOC CON FOR D. SHERWOOD

DEPARTMENT OF ENERGY
LIBRARY ROOM G-042
WASHINGTON, D.C. 20545
01CY ATTN DOC CON FOR A. LABOWITZ

EG&G, INC.
LOS ALAMOS DIVISION
P. O. BOX 809
LOS ALAMOS, NM 85544
01CY ATTN DOC CON FOR J. BREEDLOVE

UNIVERSITY OF CALIFORNIA
LAWRENCE LIVERMORE LABORATORY
P. O. BOX 808
LIVERMORE, CA 94550
01CY ATTN DOC CON FOR TECH INFO DEPT
01CY ATTN DOC CON FOR L-389 R. OTT
01CY ATTN DOC CON FOR L-31 R. HAGER
01CY ATTN DOC CON FOR L-46 F. SEWARD

LOS ALAMOS SCIENTIFIC LABORATORY
P. O. BOX 1663
LOS ALAMOS, NM 87545
01CY ATTN DOC CON FOR J. WOLCOTT
01CY ATTN DOC CON FOR R. F. TASCHEK
01CY ATTN DOC CON FOR E. JONES
01CY ATTN DOC CON FOR J. MALIK
01CY ATTN DOC CON FOR R. JEFFRIES
01CY ATTN DOC CON FOR J. ZINN
01CY ATTN DOC CON FOR P. KEATON
01CY ATTN DOC CON FOR D. WESTERVELT

SANDIA LABORATORIES
P. O. BOX 5800
ALBUQUERQUE, NM 87115
01CY ATTN DOC CON FOR J. MARTIN
01CY ATTN DOC CON FOR W. BROWN
01CY ATTN DOC CON FOR A. THORNBROUGH
01CY ATTN DOC CON FOR T. WRIGHT
01CY ATTN DOC CON FOR D. DAHLGREN
01CY ATTN DOC ON FOR 3141
01CY ATTN DOC CON FOR SPACE PROJECT DIV

SANDIA LABORATORIES
LIVERMORE LABORATORY
P. O. BOX 969
LIVERMORE, CA 94550
01CY ATTN DOC CON FOR B. MURPHEY
01CY ATTN DOC CON FOR T. COOK

OFFICE OF MILITARY APPLICATION
DEPARTMENT OF ENERGY
WASHINGTON, D.C. 20545
01CY ATTN DOC CON FOR J. GALE

OTHER GOVERNMENT

CENTRAL INTELLIGENCE AGENCY
ATTN RD/SI, RM 5G48, HQ BLDG
WASHINGTON, D.C. 20505
01CY ATTN OSI/PSID RM 5F 19

DEPARTMENT OF COMMERCE
NATIONAL BUREAU OF STANDARDS
WASHINGTON, D.C. 20234
(ALL CORRES: ATTN SEC OFFICER FOR)
01CY ATTN R. MOORE

INSTITUTE FOR TELECOM SCIENCES
NATIONAL TELECOMMUNICATIONS & INFO ADMIN
BOULDER, CO 80303
01CY ATTN A. JEAN (UNCLASS ONLY)
01CY ATTN W. UTLAUT
01CY ATTN D. CROMBIE
01CY ATTN L. BERRY

NATIONAL OCEANIC & ATMOSPHERIC ADMIN
ENVIRONMENTAL RESEARCH LABORATORIES
DEPARTMENT OF COMMERCE
BOULDER, CO 80302
01CY ATTN R. GRUBB
01CY ATTN AERONOMY LAB G. REID

AEROSPACE CORPORATION
P. O. BOX 92957
LOS ANGELES, CA 90009
01CY ATTN I. GARFUNKEL
01CY ATTN T. SALMI
01CY ATTN V. JOSEPHSON
01CY ATTN S. BOWER
01CY ATTN N. STOCKWELL
01CY ATTN D. OLSEN
01CY ATTN J. CARTER
01CY ATTN F. MORSE
01CY ATTN SMFA FOR PWW

ANALYTICAL SYSTEMS ENGINEERING CORP
5 OLD CONCORD ROAD
BURLINGTON, MA 01803
01CY ATTN RADIO SCIENCES

BERKELEY RESEARCH ASSOCIATES, INC.
P. O. BOX 983
BERKELEY, CA 94701
01CY ATTN J. WORKMAN

BOEING COMPANY, THE
P. O. BOX 3707
SEATTLE, WA 98124
01CY ATTN G. KEISTER
01CY ATTN D. MURRAY
01CY ATTN G. HALL
01CY ATTN J. KENNEY

CALIFORNIA AT SAN DIEGO, UNIV OF
IPAPS, B-019
LA JOLLA, CA 92093
01CY ATTN HENRY G. BOOKER

BROWN ENGINEERING COMPANY, INC.
CUMMINGS RESEARCH PARK
HUNTSVILLE, AL 35807
01CY ATTN ROMEO A. DELIBERIS

CHARLES STARK DRAPER LABORATORY, INC.
555 TECHNOLOGY SQUARE
CAMBRIDGE, MA 02139
01CY ATTN D. B. COX
01CY ATTN J. P. GILMORE

COMPUTER SCIENCES CORPORATION
6565 ARLINGTON BLVD
FALLS CHURCH, VA 22046
01CY ATTN H. BLANK
01CY ATTN JOHN SPOOR
01CY ATTN C. NAIL

COMSAT LABORATORIES
LINTHICUM ROAD
CLARKSBURG, MD 20734
01CY ATTN G. HYDE

CORNELL UNIVERSITY
DEPARTMENT OF ELECTRICAL ENGINEERING
ITHACA, NY 14850
01CY ATTN D. T. FARLEY JR

ELECTROSPACE SYSTEMS, INC.
BOX 1359
RICHARDSON, TX 75080
01CY ATTN H. LOGSTON
01CY ATTN SECURITY (PAUL PHILLIPS)

ESL INC.
495 JAVA DRIVE
SUNNYVALE, CA 94086
01CY ATTN J. ROBERTS
01CY ATTN JAMES MARSHALL
01CY ATTN C. W. PRETTIE

FORD AEROSPACE & COMMUNICATIONS CORP
3939 FABIAN WAY
PALO ALTO, CA 94303
01CY ATTN J. T. MATTINGLEY

GENERAL ELECTRIC COMPANY
SPACE DIVISION
VALLEY FORGE SPACE CENTER
GODDARD BLVD KING OF PRUSSIA
P. O. BOX 8555
PHILADELPHIA, PA 19101
01CY ATTN M. H. BORTNER SPACE SCI LAB

GENERAL ELECTRIC COMPANY
P. O. BOX 1122
SYRACUSE, NY 13201
01CY ATTN F. REIBERT

GENERAL ELECTRIC COMPANY
TEMPO-CENTER FOR ADVANCED STUDIES
816 STATE STREET (P.O. DRAWER QQ)
SANTA BARBARA, CA 93102
01CY ATTN DASIAC
01CY ATTN DON CHANDLER
01CY ATTN TOM BARRETT
01CY ATTN TIM STEPHANS
01CY ATTN WARREN S. KNAPP
01CY ATTN WILLIAM MCNAMARA
01CY ATTN B. GAMBILL
01CY ATTN MACK STANTON

GENERAL ELECTRIC TECH SERVICES CO., INC.
ATTN
COURT STREET
SYRACUSE, NY 13201
01CY ATTN G. MILLMAN

GENERAL RESEARCH CORPORATION
SANTA BARBARA DIVISION
P. O. BOX 6770
SANTA BARBARA, CA 93111
01CY ATTN JOHN ISE JR
01CY ATTN JOEL GARBARINO

GEOPHYSICAL INSTITUTE
UNIVERSITY OF ALASKA
FAIRBANKS, AK 99701
(ALL CLASS ATTN: SECURITY OFFICER)
01CY ATTN T. N. DAVIS (UNCL ONLY)
01CY ATTN NEAL BROWN (UNCL ONLY)
01CY ATTN TECHNICAL LIBRARY

GTE SYLVANIA, INC.
ELECTRONICS SYSTEMS GRP-EASTERN DIV
77 A STREET
NEEDHAM, MA 02194
01CY ATTN MARSHAL CROSS

ILLINOIS, UNIVERSITY OF
DEPARTMENT OF ELECTRICAL ENGINEERING
URBANA, IL 61803
01CY ATTN K. YEH

ILLINOIS, UNIVERSITY OF
107 COBLE HALL
801 S. WRIGHT STREET
URBANA, IL 60680
(ALL CORRES ATTN SECURITY SUPERVISOR FOR)
01CY ATTN K. YEH

INSTITUTE FOR DEFENSE ANALYSES
400 ARMY-NAVY DRIVE
ARLINGTON, VA 22202
01CY ATTN J. M. AEIN
01CY ATTN ERNEST BAUER
01CY ATTN HANS WOLFHARD
01CY ATTN JOEL BENGSTON

HSS, INC.
2 ALFRED CIRCLE
BEDFORD, MA 01730
01CY ATTN DONALD HANSEN

INTL TEL & TELEGRAPH CORPORATION
500 WASHINGTON AVENUE
NUTLEY, NJ 07110
01CY ATTN TECHNICAL LIBRARY

JAYCOR
1401 CAMINO DEL MAR
DEL MAR, CA 92014
01CY ATTN S. R. GOLDMAN

JOHNS HOPKINS UNIVERSITY
APPLIED PHYSICS LABORATORY
JOHNS HOPKINS ROAD
LAUREL, MD 20810
01CY ATTN DOCUMENT LIBRARIAN
01CY ATTN THOMAS POTEMRA
01CY ATTN JOHN DASSOULAS

LOCKHEED MISSILES & SPACE CO INC
P. O. BOX 504
SUNNYVALE, CA 94088
01CY ATTN DEPT 60-12
01CY ATTN D. R. CHURCHILL

LOCKHEED MISSILES AND SPACE CO INC
3251 HANOVER STREET
PALO ALTO, CA 94304
01CY ATTN MARTIN WALT DEPT 52-10
01CY ATTN RICHARD G. JOHNSON DEPT 52-12
01CY ATTN W. L. IMHOF DEPT 52-12

KAMAN SCIENCES CORP
P. O. BOX 7463
COLORADO SPRINGS, CO 80933
01CY ATTN T. MEAGHER

LINKABIT CORP
10453 ROSELLE
SAN DIEGO, CA 92121
01CY ATTN IRWIN JACOBS

M.I.T. LINCOLN LABORATORY
P. O. BOX 73
LEXINGTON, MA 02173
01CY ATTN DAVID M. TOWLE
01CY ATTN P. WALDRON
01CY ATTN L. LOUGHLIN
01CY ATTN D. CLARK

MARTIN MARIETTA CORP
ORLANDO DIVISION
P. O. BOX 5837
ORLANDO, FL 32805
01CY ATTN R. HEFFNER

MCDONNELL DOUGLAS CORPORATION
5301 BOLSA AVENUE
HUNTINGTON BEACH, CA 92647
01CY ATTN N. HARRIS
01CY ATTN J. MOULE
01CY ATTN GEORGE MROZ
01CY ATTN W. OLSON
01CY ATTN R. W. HALPRIN
01CY ATTN TECHNICAL LIBRARY SERVICES

MISSION RESEARCH CORPORATION
735 STATE STREET
SANTA BARBARA, CA 93101
01CY ATTN P. FISCHER
01CY ATTN W. F. CREVIER
01CY ATTN STEVEN L. GUTSCHE
01CY ATTN D. SAPPENFIELD
01CY ATTN R. BOGUSCH
01CY ATTN R. HENDRICK
01CY ATTN RALPH KILB
01CY ATTN DAVE SOWLE
01CY ATTN F. FAJEN
01CY ATTN M. SCHEIBE
01CY ATTN CONRAD L. LONGMIRE
01CY ATTN WARREN A. SCHLUETER

MITRE CORPORATION, THE
P. O. BOX 208
BEDFORD, MA 01730
01CY ATTN JOHN MORGANSTERN
01CY ATTN G. HARDING
01CY ATTN C. E. CALLAHAN

MITRE CORP
WESTGATE RESEARCH PARK
1820 DOLLY MADISON BLVD
MCLEAN, VA 22101
01CY ATTN W. HALL
01CY ATTN W. FOSTER

PACIFIC-SIERRA RESEARCH CORP
1456 CLOVERFIELD BLVD.
SANTA MONICA, CA 90404
01CY ATTN E. C. FIELD JR

PENNSYLVANIA STATE UNIVERSITY
IONOSPHERE RESEARCH LAB
318 ELECTRICAL ENGINEERING EAST
UNIVERSITY PARK, PA 16802
(NO CLASSIFIED TO THIS ADDRESS)
01CY ATTN IONOSPHERIC RESEARCH LAB

PHOTOMETRICS, INC.
442 MARRETT ROAD
LEXINGTON, MA 02173
01CY ATTN IRVING L. KOFSKY

PHYSICAL DYNAMICS INC.
P. O. BOX 3027
BELLEVUE, WA 98009
01CY ATTN E. J. FREMOUW

PHYSICAL DYNAMICS INC.
P. O. BOX 1069
BERKELEY, CA 94701
01CY ATTN A. THOMPSON

R & D ASSOCIATES
P. O. BOX 9695
MARINA DEL REY, CA 90291
01CY ATTN FORREST GILMORE
01CY ATTN BRYAN GABBARD
01CY ATTN WILLIAM B. WRIGHT JR
01CY ATTN ROBERT F. LELEVIER
01CY ATTN WILLIAM J. KARZAS
01CY ATTN H. ORY
01CY ATTN C. MACDONALD
01CY ATTN R. TURCO

RAND CORPORATION, THE
1700 MAIN STREET
SANTA MONICA, CA 90406
01CY ATTN CULLEN CRAIN
01CY ATTN ED BEDROZIAN

RIVERSIDE RESEARCH INSTITUTE
80 WEST END AVENUE
NEW YORK, NY 10023
01CY ATTN VINCE TRAPANI

SCIENCE APPLICATIONS, INC.
P. O. BOX 2351
LA JOLLA, CA 92038
01CY ATTN LEWIS M. LINSON
01CY ATTN DANIEL A. HAMLIN
01CY ATTN D. SACHS
01CY ATTN E. A. STRAKER
01CY ATTN CURTIS A. SMITH
01CY ATTN JACK MCDOUGALL

RAYTHEON CO.
528 BOSTON POST ROAD
SUDBURY, MA 01776
01CY ATTN BARBARA ADAMS

SCIENCE APPLICATIONS, INC.
HUNTSVILLE DIVISION
2109 W. CLINTON AVENUE
SUITE 700
HUNTSVILLE, AL 35805
01CY ATTN DALE H. DIVIS

SCIENCE APPLICATIONS, INCORPORATED
8400 WESTPARK DRIVE
MCLEAN, VA 22101
01CY ATTN J. COCKAYNE

SCIENCE APPLICATIONS, INC.
80 MISSION DRIVE
PLEASANTON, CA 94566
01CY ATTN SZ

SRI INTERNATIONAL
333 RAVENSWOOD AVENUE
MENLO PARK, CA 94025
01CY ATTN DONALD NEILSON
01CY ATTN ALAN BURNS
01CY ATTN G. SMITH
01CY ATTN L. L. COBB
01CY ATTN DAVID A. JOHNSON
01CY ATTN WALTER G. CHESNUT
01CY ATTN CHARLES L. RINO
01CY ATTN WALTER JAYE
01CY ATTN M. BARON
01CY ATTN RAY L. LEADABRAND
01CY ATTN G. CARPENTER
01CY ATTN G. PRICE
01CY ATTN J. PETERSON
01CY ATTN R. MAKE, JR.
01CY ATTN V. GONZALES
01CY ATTN D. MCDANIEL

TECHNOLOGY INTERNATIONAL CORP
75 WIGGINS AVENUE
BEDFORD, MA 01730
01CY ATTN W. P. BOQUIST

TRW DEFENSE & SPACE SYS GROUP
ONE SPACE PARK
REDONDO BEACH, CA 90278
01CY ATTN R. K. PLEBUCH
01CY ATTN S. ALTSCHULER
01CY ATTN D. DEE

VISIDYNE, INC.
19 THIRD AVENUE
NORTH WEST INDUSTRIAL PARK
BURLINGTON, MA 01803
01CY ATTN CHARLES HUMPHREY
01CY ATTN J. W. CARPENTER

IONOSPHERIC MODELING DISTRIBUTION LIST
UNCLASSIFIED ONLY

PLEASE DISTRIBUTE ONE COPY TO EACH OF THE FOLLOWING PEOPLE:

ADVANCED RESEARCH PROJECTS AGENCY (ARPA)
STRATEGIC TECHNOLOGY OFFICE
ARLINGTON, VIRGINIA

CAPT. DONALD M. LEVINE

NAVAL RESEARCH LABORATORY
WASHINGTON, D.C. 20375

DR. P. MANGE
DR. R. MEIER
DR. E. SZUSZCZEWICZ - CODE 7127

DR. J. GOODMAN - CODE 7560

SCIENCE APPLICATIONS, INC.
1250 PROSPECT PLAZA
LA JOLLA, CALIFORNIA 92037

DR. D. A. HAMLIN
DR. L. LINSON
DR. D. SACHS

DIRECTOR OF SPACE AND ENVIRONMENTAL LABORATORY
NOAA
BOULDER, COLORADO 80302

DR. A. GLENN JEAN
DR. G. W. ADAMS
DR. D. N. ANDERSON
DR. K. DAVIES
DR. R. F. DONNELLY

A. F. GEOPHYSICS LABORATORY
L. G. HANSOM FIELD
BEDFORD, MASS. 01730

DR. T. EUKINS
DR. W. SWIDER
MRS. R. SAGALYN
DR. J. M. FORBES
DR. T. J. KENESHEA
DR. J. AARONS

OFFICE OF NAVAL RESEARCH
800 NORTH QUINCY STREET
ARLINGTON, VIRGINIA 22217

DR. H. MULLANEY

COMMANDER
NAVAL ELECTRONICS LABORATORY CENTER
SAN DIEGO, CALIFORNIA 92152

DR. M. BLEIWEISS
DR. I. ROTHMULLER
DR. V. HILDEBRAND
MR. R. ROSE

U. S. ARMY ABERDEEN RESEARCH AND DEVELOPMENT CENTER
BALLISTIC RESEARCH LABORATORY
ABERDEEN, MARYLAND

DR. J. HEIMERL

COMMANDER
NAVAL AIR SYSTEMS COMMAND
DEPARTMENT OF THE NAVY
WASHINGTON, D.C. 20360

DR. T. CZUBA

HARVARD UNIVERSITY
HARVARD SQUARE
CAMBRIDGE, MASS. 02138

DR. M. B. MCELROY
DR. R. LINDZEN

PENNSYLVANIA STATE UNIVERSITY
UNIVERSITY PARK, PENNSYLVANIA 16802

DR. J. S. NISBET
DR. P. R. ROHRBAUGH
DR. D. E. BARAN
DR. L. A. CARPENTER
DR. M. LEE
DR. R. DIVANY
DR. P. BENNETT
DR. E. KLEVANS

UNIVERSITY OF CALIFORNIA, LOS ANGELES
405 HILLGARD AVENUE
LOS ANGELES, CALIFORNIA 90024

DR. F. V. CORONITI
DR. C. KENNEL

UNIVERSITY OF CALIFORNIA, BERKELEY
BERKELEY, CALIFORNIA 94720

DR. M. HUDSON

UTAH STATE UNIVERSITY
4TH N. AND 8TH STREETS
LOGAN, UTAH 84322

DR. P. M. BANKS
DR. R. HARRIS
DR. V. PETERSON
DR. R. MEGILL
DR. K. BAKER

CORNELL UNIVERSITY
ITHACA, NEW YORK 14850

DR. W. E. SWARTZ
DR. R. SUDAN
DR. D. FARLEY
DR. M. KELLEY

NASA
GODDARD SPACE FLIGHT CENTER
GREENBELT, MARYLAND 20771

DR. S. CHANDRA
DR. K. MAEDO

PRINCETON UNIVERSITY
PLASMA PHYSICS LABORATORY
PRINCETON, NEW JERSEY 08540

DR. F. PERKINS
DR. E. FRIEMAN

INSTITUTE FOR DEFENSE ANALYSIS
400 ARMY/NAVY DRIVE
ARLINGTON, VIRGINIA 22202

DR. E. BAUER

UNIVERSITY OF PITTSBURGH
PITTSBURGH, PA. 15213

DR. N. ZABUSKY
DR. M. BIONDI